POLITECNICO DI TORINO



Master Degree course in Automotive Engineering

Master Degree Thesis

Comparison of Cooling Circuit in Electric motors for Automobiles

Supervisors

Prof. ANDREA TONOLI PhD Candidate. CHENGYANG YE

> Candidate LIWEI HE

ACADEMIC YEAR 2025-2026

Acknowledgements

I am deeply grateful to my supervisor, Professor Andrea Tonoli, for offering me the opportunity to work with him and for his unwavering help, guidance, and support. His advice and insights have been instrumental in the completion of this thesis.

I also really appreciate to all my colleagues at Politecnico di Torino, who generously shared valuable insights and practical suggestions related to my studies. Specially Mr. Yu Huang gave me invaluable life advice and Mr. Zexuan Lin gave me selfless academic guidance and support throughout my studies. I would also like to give special acknowledgment to PhD candidate Chenyang Ye, who patiently guided me step by step and provided invaluable support throughout this thesis.

Finally, I would like to convey my heartfelt gratitude to my family, whose encouragement and support enabled me to pursue my studies at Politecnico di Torino. I am also thankful to all my friends in China, who kindly supported me. Additionally, I acknowledge the growth fostered by the challenges I encountered, and I am grateful to myself for persisting through difficult times.

Abstract

Motor cooling systems are crucial to the performance and reliability of electric vehicles. In this work, three different oil cooling circuit configurations for an Interior Permanent Magnet(IPM)motor were designed and evaluated through computational fluid dynamics(CFD) simulations. The proposed cases include: (i)case.1: coolant flowing through a hollow shaft; (ii)case.2: cooling channels embedded in the shaft and rotor laminations; and (iii)case.3: cooling channels embedded in the gaps between the shaft and rotor laminations and the magnets.

The interior permanent magnet synchronous motor chosen in this paper features a uniformly distributed structure, with repetitive geometry and flow patterns. To simplify the model and reduce computational complexity, a sector-shaped region, one-eighth of the motor, is used as the computational domain to represent the entire motor. The anisotropic thermal characteristics of the stator winding, the equivalence of the rotor and air gap regions, and the stator water cooling jacket are all considered, forming the core methodology of this study. The winding is treated as a single entity with anisotropic behavior. The winding is composed of copper and non-copper materials, or insulators. All non-copper materials are treated as equivalent homogeneous media. The equivalent axial thermal conductivity is calculated to be $343.286W/(m*^{\circ}C)$ and the equivalent radial thermal conductivity is calculated to be $1.454W/(m *^{\circ} C)$ of the winding are calculated, and the winding entity is configured. The frozen rotor method is used to convert the transient rotation into a steady-state problem. A rotational speed of 16,000 rpm is applied to the rotor lamination surface to simulate motor rotation. The air gap region is modeled by modeling the air gap between the rotor and stator laminations, and the wall material and thickness of the air gap between the rotor laminations and the magnets are defined in ANSYS FLUENT. The stator water cooling jacket is equivalently calculated using equations to calculate the equivalent heat transfer coefficient to be $1873.044W/(m*^{\circ}C)$, and the housing wall is defined. After the simulation is completed, simulation results such as the maximum temperature distribution, maximum pressure, and residual plots of each component are obtained to verify model convergence and cooling performance. Finally, electromagnetic analysis is performed to verify the impact of different cooling circuits on the electromagnetic performance of the motor.

The results show that of the three designs, the third configuration offers the most effective cooling, significantly reducing winding and rotor temperatures. Placing the coolant closer to the heat source can more effectively reduce rotor temperature; however, the associated complexity of the piping system results in a greater pressure drop. Furthermore, due to the inherently low thermal conductivity of air within the air gap, changes in the rotor cooling strategy have minimal impact on the cooling performance. Furthermore, it does not adversely affect the motor's electromagnetic characteristics. This study highlights the importance of optimizing cooling design for improving the thermal performance of automotive IPM motors.

Keywords: IPM motor, CFD simulations, Cooling circuit, Electromagnetic

Contents

1	Introduction									
	1.1	Backgr	round							
	1.2	Motiva	ation							
	1.3	Thesis	outline							
2	The	Pheoretical Background 9								
	2.1	Fundamentals of Electrical Motor Theory								
	2.2		mentals of Heat Transfer Theory							
	2.3									
		2.3.1	CFD simulation							
		2.3.2	Analytical modeling technique							
	2.4	re Technical Support								
		2.4.1	Motor CAD							
		2.4.2	CATIA							
		2.4.3	ANSYS							
	2.5	iew of cooling strategy								
		2.5.1	Natural Passive Cooling							
		2.5.2	Forced Air							
		2.5.3	Housing water jacket							
		2.5.4	Stator cooling							
		2.5.5	Rotor cooling							
		2.5.6	Phase change							
3	Met	thodolo	ogy 23							
	3.1	Design	of cooling strategies							
		3.1.1	Case 1							
		3.1.2	Case 2							
		3.1.3	Case 3							
	3.2	Set-up	of model							
	3.3	alence of components								
		3.3.1	Equivalence of the Winding							
		3.3.2	Equivalence of the Rotor and Air-gap							
		3.3.3	Equivalence of the Stator Water Jacket							
	3.4	Selecti	on of operating point							

4	Results								
	4.1	Convergence of the model	39						
	4.2	Temperature	42						
	4.3	Pressure	44						
	4.4	Electric-magnetic analysis	46						
5	Conclusion and future work								
	5.1	Conclusion	49						
	5.2	Future work	49						
Li	st of	Figures	51						
Bi	ibliog	graphy	53						



Chapter 1

Introduction

1.1 Background

Against the backdrop of increasingly severe global climate change and environmental degradation, environmental protection has become a global issue of common concern. Transportation is a major source of carbon emissions and air pollution.

According to the US Alternative Fuels Data Center (AFDC), pure electric vehicles have no tailpipe emissions during use, while greenhouse gas emissions mainly depend on the source of electricity provided to the electric vehicles [8]. The US Environmental Protection Agency (EPA) further emphasized that, taking into account power generation emissions, the greenhouse gas emissions of electric vehicles are generally still lower than those of similar fuel vehicles [9]. Therefore, the development of pure electric vehicles is the mainstream trend in the future.

In Europe, research by the Transport and Environment Organization shows that electric vehicles have emissions that are more than three times lower than gasoline vehicles throughout their life cycle; the latest research even points out that in the European market, electric vehicles can reduce carbon emissions by 73% over their life cycle compared to fuel vehicles [6]. The European Environment Agency also pointed out that greenhouse gas emissions from electric vehicles are 17 - 30% lower than those of fuel vehicles, depending on the power structure [2]. The data fully demonstrates that under most power conditions, electric vehicles have significant emission reduction advantages over fuel vehicles.

In China, the new energy vehicle industry has developed rapidly in recent years. In the first half of 2025, Chinese new energy vehicle production and sales reached 6.968 million and 6.937 million respectively, up more than 40% year-on-year, accounting for 44.3% of total new vehicle sales [5]. Among them, the growth in production and sales of pure electric vehicles was particularly prominent. In May alone, the production and sales reached 820,000 and 834,000 respectively, up more than 40% year-on-year [4]. This data shows that China has become the major market of world for new energy vehicles, and electric vehicles are gradually moving from policy promotion to market popularization.

The advantages of electric vehicles are reflected in many aspects. First, there is a significant emission reduction effect. As the proportion of renewable energy in the power

structure continues to increase, electric vehicles can achieve almost zero emissions during operation, which is of great significance to improving urban air quality and responding to climate change. Second, electric vehicles reduce dependence on oil, optimize the energy consumption structure, and improve energy security. In addition, electric vehicles have also promoted the development of emerging industries such as battery manufacturing, recycling, intelligent networking and charging facilities, injecting new momentum into economic transformation and upgrading.

Overall, new energy vehicles, especially pure electric vehicles, are an important technical path for the world to respond to environmental pollution and climate change. Driven by government policies, technological advancements, and expanding market demand, electric vehicles will play a more important role in the future. With breakthroughs in battery technology, improved recycling systems, and a cleaner power mix, the environmental benefits of electric vehicles throughout their life cycle will be further enhanced. They represent more than just a revolutionary form of transportation; they also play a key role in energy transformation, industrial upgrading, and green development. Among the core technologies of new energy vehicles, the drive motor plays a crucial role. It directly determines the power performance of vehicle, energy efficiency, and reliability. With the rapid development of the new energy vehicle industry, technological advancements and industrial development of drive motors have become key areas of focus for global automakers and supply chain companies.

The drive motor is a key component that converts electrical energy into mechanical energy, providing driving force for the wheels of vehicle. Unlike traditional fuel-powered vehicles, which rely on engines to burn gasoline or diesel for power, electric vehicles are primarily powered by batteries and motors. The battery stores electrical energy, while the motor converts it into torque and speed, thereby driving the vehicle. The performance of the drive motor, including power density, efficiency, peak torque, volume-to-weight ratio, cost, and reliability, directly impacts an electric acceleration of vehicle, range, and overall user experience. Currently, the most widely used drive motors in new energy vehicles are mainly the following types: DC motors, AC induction motors, permanent magnet synchronous motors, and switched reluctance motors. This article focuses on IPM motors, which generally refer to internal permanent magnet synchronous motors (IPMs). IPM motors utilize permanent magnets as the rotor excitation source. These magnets are embedded within the rotor to achieve high performance and efficiency. They are widely used in electric vehicles, robotics, and other fields. IPM motors have the following features:

- Internal permanent magnets: Unlike surface permanent magnet synchronous motors (SPMs), which mount permanent magnets on the exterior of rotor, IPM motors embed permanent magnets within the rotor.
- High efficiency and high power density: Through a clever structural design, IPM motors achieve higher efficiency and power density, and offer improved performance at high speeds.
- Wide speed range: They enable a wider speed range and provide strong torque even at low speeds.

• In conjunction with a servo drive: IPM motors are typically used in conjunction with a frequency converter or servo drive, which uses power electronics technology to precisely control the AC signal to achieve efficient and smooth operation.

1.2 Motivation

In the future, the development of drive motors will be closely aligned with the overall trajectory of new energy vehicles (NEVs). On one hand, motor performance is expected to advance toward higher efficiency, compact structures, and reduced cost. On the other hand, the integrated optimization of motors, electronic control units, and battery systems will become increasingly critical, with intelligent electric drive systems emerging as the mainstream solution. Moreover, as the adoption of NEVs accelerates, research on the recycling, reuse, and green manufacturing of drive motors will gain growing importance.

As one of the core technologies of NEVs, the drive motor plays a decisive role in determining the competitiveness of the industry. Enterprises that secure advantages in motor technology, industrialization, and supply chain robustness will be better positioned to gain strategic leadership in the evolving NEV landscape. Among various motor types, interior permanent magnet (IPM) motors offer high efficiency and excellent power density, making them particularly suitable for electric vehicle (EV) applications. During operation, however, electromagnetic, mechanical, and stray losses in motor components inevitably generate heat. This thermal energy is transferred to the cooling medium via conduction, convection, and/or radiation, depending on the temperature gradient between heat sources and sinks.

To address these challenges, this study proposes a rotor cooling strategy based on a hollow-shaft design that enables coolant circulation. In particular, oil cooling has attracted significant research attention due to its favorable thermal and electrical insulation properties. By integrating cooling channels within the rotor, oil can achieve direct thermal contact with the rotor laminations or with ferromagnetic elements, thereby enhancing heat dissipation efficiency. Within this framework, three rotor oil-cooling configurations of varying complexity and performance are comparatively analyzed for EV powertrain applications.

The primary contribution of this work lies in its systematic technical evaluation of alternative rotor oil-cooling designs for IPM motors, providing insights into their respective advantages, limitations, and potential for future implementation in high-performance electric drives.

1.3 Thesis outline

This paper is organized as follows:

- Chapter 2 details explanation of the theoretical basis of this paper.
- Chapter 3 introduces the simulation methodologies.
- Chapter 4 presents simulation results and discusses the cooling performance of different solutions.

• Chapter 5 provides final conclusion and future work.

Chapter 2

Theoretical Background

2.1 Fundamentals of Electrical Motor Theory

This paper focuses on interior permanent magnet (IPM) motors, which serve as the core power source for EVs. The IPM motor structure is composed of a stator, rotor, windings, permanent magnets, and auxiliary systems such as cooling and sensing units. The stator typically consists of a laminated core fabricated from cold-rolled silicon steel sheets, with copper enameled windings embedded within its slots. When energized by a three-phase current, these windings generate a rotating magnetic field that drives motor operation.

The rotor consists of a laminated iron core, an alloy steel shaft, and embedded permanent magnets, typically made of high-performance sintered Neodymium–Iron–Boron material. These permanent magnets provide a strong magnetic field, enabling high torque density, while also contributing to the generation of electromagnetic torque through synergistic action with the rotor's reluctance effect. To withstand the mechanical stresses and thermal loads associated with high-speed operation, the magnets are reinforced with epoxy potting, glass fiber tape, or carbon fiber sleeves. The motor housing, typically constructed of aluminum alloy, provides structural support for the stator and houses thermal management systems, such as water cooling jackets or oil cooling channels, to dissipate heat from the windings and magnets during high-power operation. Auxiliary components, including high-speed bearings, temperature sensors, and position sensors, further ensure operational reliability and safety.

Due to its high power density, excellent field-weakening capability, and superior efficiency, the IPM motor has become the dominant driving solution in NEVs. Compared with induction motors, IPM motors offer advantages in terms of torque density, efficiency, and performance in the high-speed range. Nevertheless, they also present manufacturing challenges, requiring precise lamination stacking, magnet fastening, and potting techniques.

2.2 Fundamentals of Heat Transfer Theory

The law of conservation of energy states that the input electrical energy of motor, P_{in} , is divided into output mechanical power, P_{out} , and various power losses, P_{loss} . Losses

ultimately manifest themselves as heat:

$$P_{in} = P_{out} + P_{loss}, \quad Q = P_{loss} \cdot t \tag{2.1}$$

Heat Q accumulates over operating time, causing the temperature of motor to rise. Heat conduction law: Heat from within a motor is conducted outward through the stator core, windings, and housing:

$$q = -\lambda \frac{dT}{dx} \tag{2.2}$$

Where λ is the thermal conductivity, and dT/dx is the temperature gradient.

Convection and Radiation: Heat from the motor surface dissipates to the air through natural or forced convection, with some radiation also occurring.

$$Q_{conv} = hA(T_s - T_{\infty}), \quad Q_{rad} = \epsilon \sigma A(T_s^4 - T_{\infty}^4)$$
(2.3)

Here, h is the convective heat transfer coefficient, and ϵ is the surface radiation coefficient.

The root causes of heat generation during motor operation can be understood from the perspectives of energy conversion and loss. Not all input electrical energy is converted into mechanical energy, a portion is released as heat. These losses primarily include copper loss, iron loss, mechanical loss, and stray loss. Copper loss is Joule heating generated by the conductor resistance when current flows through the rotor windings:

$$P_{cu} = I^2 R (2.4)$$

For small temperature variations, the thermal conductivity can be approximated linearly:

$$\lambda(T) = \lambda_0 (1 + \alpha(T - T_0)), \tag{2.5}$$

where λ_0 is the reference thermal conductivity at temperature T_0 , and α is the temperature coefficient.

The equation of thermal resistance $R_{\rm th}$ is:

$$R_{\rm th}(T) = \frac{L}{A \lambda_0 (1 + \alpha (T - T_0))}.$$
 (2.6)

The core of motor, exposed to an alternating magnetic field, generates two types of losses: hysteresis loss and eddy current loss. Hysteresis loss refers to the energy dissipated by the repeated switching of magnetic domains and is proportional to the flux density and frequency. Eddy current loss refers to the heat generated by the alternating magnetic flux in the core due to circulating currents. Mechanical losses include energy losses caused by bearing friction, windage, and other mechanical friction. Stray losses, caused by magnetic flux leakage and harmonic effects, although a smaller proportion, are not negligible in high-efficiency motors.

2.3 Simulation Methodologies

The heat generated by electric vehicle motors during operation directly impacts efficiency, reliability, and service life. To predict temperature rise and optimize heat dissipation structures, various modeling and simulation methods are often employed. Currently, the most widely used technologies include Computational fluid dynamics (CFD)simulation, and analytical modeling techniques. This article will compare and analyze the principles, characteristics, and applications of these two methods. CFD simulation and analytical modeling techniques each have their own strengths and weaknesses, but they complement each other in electric vehicle motor thermal analysis. Properly selecting and combining these two methods can achieve an optimal balance between design efficiency and result accuracy, providing theoretical support for efficient heat dissipation and reliable operation of the motor.

2.3.1 CFD simulation

Numerical simulation enables the calculation of electromagnetic, thermal, and structural fields in electric motors by employing numerical discretization techniques such as the finite element method (FEM) and finite volume method (FVM). The core principle involves discretizing the motor geometry into grid cells and solving the governing equations of electromagnetics, heat conduction, or coupled multiphysics phenomena within each cell. The main advantages of numerical simulation lie in its ability to accurately model complex motor geometries and heterogeneous material properties. It provides precise estimation of stator winding copper losses, iron loss distribution, and heat conduction pathways, while also allowing for coupled electromagnetic—thermal analyses to capture multi-physics interactions. However, its drawbacks include significant computational cost and long simulation time, making it highly dependent on computing resources and less suitable for rapid engineering optimization. In practice, numerical simulation is widely applied to motor loss distribution analysis, temperature rise prediction, and design verification, offering valuable insights to support the development of high-performance and reliable electric drive systems.

CFD simulation is a widely used numerical method, particularly suited for analyzing motor cooling systems and external flow fields. It is primarily employed to investigate heat convection and dissipation mechanisms, which are especially critical for liquid-cooled, oil-cooled, and air-cooled electric motors. The underlying principle is to simulate fluid flow and heat transfer of the cooling medium by solving the Navier–Stokes equations in conjunction with the energy equation. CFD offers several advantages. It can intuitively capture coolant velocity distributions, temperature fields, and pressure fields, thereby providing insights into the effectiveness of thermal management systems. It also enables optimization of cooling channels, pump flow rates, and radiator structures, and when coupled with heat source distribution, it provides highly accurate predictions of motor temperature fields. Nonetheless, CFD has notable limitations: the results are sensitive to meshing quality and boundary condition settings; three-dimensional transient simulations often demand substantial computational resources and extended run times; and the method requires users to possess a solid foundation in fluid mechanics and numerical

analysis, which poses a steep learning curve for beginners. In practice, CFD simulation is commonly applied in liquid-cooled motor stator winding thermal design, oil-cooled rotor bearing temperature control, and radiator structure optimization, thereby playing a crucial role in the development of advanced motor cooling technologies.

This article primarily uses ANSYS FLUENT software, based on CFD simulation methods. Common CFD turbulence models are categorized and represented as algebraic, one-equation, two-equation, Reynolds stress, large eddy simulation, and detached eddy simulation. The algebraic model assumes that turbulent viscosity is related to the local velocity gradient and mixing length. It is simple and computationally inefficient, but has limited accuracy. This model is applicable to low Reynolds numbers and simple boundary layer flows. The one-equation model solves a transport equation for the turbulent viscosity coefficient. It is computationally efficient and effective in simulating aeronautical flows and boundary layers, and is commonly used in external flow fields and aerodynamics. The two-equation model closes the Reynolds-averaged Navier-Stokes (RANS) equations by establishing transport equations for two turbulent quantities (typically the turbulent kinetic energy k and its dissipation rate ϵ or the specific dissipation rate / frequency ω) (that is, the series of models $k-\epsilon$ and the series of models $k-\omega$. These two-equation models are widely used in engineering CFD, balancing computational efficiency with physical descriptive power. The Reynolds stress model directly solves the Reynolds stress transport equation, rather than using the turbulent viscosity assumption. This model is capable of capturing strong vortices, curvature, and secondary flows. However, its drawbacks are computational complexity and poor convergence. This model is suitable for complex flows requiring high precision, such as swirls and bends. Large eddy simulation(LES) directly analyzes large-scale turbulent eddies and models small-scale eddies. It features high accuracy and the ability to capture transient characteristics, but it is computationally expensive. It is suitable for research simulations, unsteady turbulence, combustion, and noise prediction. Detached eddy simulation (DES) is a hybrid approach combining Reynolds-averaged equations (RANS) and LES. Its characteristic is that RANS reduces computational effort in the boundary layer and LES improves accuracy in the detachment region. It is suitable for large-scale complex flows, such as aircraft external flows and automobile wakes. In this paper, a two-equation turbulence model is primarily used. Since motor cooling flows have the following characteristics:

- Complex geometry: The motor contains complex internal structures such as winding slots, narrow gaps, cooling channels, winding ends, and rotors.
- Complex flow regime: Typically, the Reynolds number is high and the flow is turbulent, often accompanied by separation, secondary flow and reattachment.
- High heat transfer requirements: Motor cooling requires not only predicting overall temperatures but also identifying local hotspots, placing high demands on heat transfer coefficient calculation accuracy.

For internal cooling channels and locally separated flows in motors, zero-equation and one-equation models often fail to provide reliable results. The two-equation model offers high versatility and offers the best accuracy/cost balance for engineering problems. It

strikes a balance between accuracy and efficiency, capturing key turbulence effects in complex geometries without requiring the computational resources of LES. Its high maturity, extensively validated model parameters and boundary treatment methods, and strong engineering reliability make it suitable for heat transfer analysis, providing reasonable heat transfer coefficients and wall friction, meeting the needs of motor hotspot prediction and cooling optimization.

The two transport equations for the standard $k - \epsilon$ are:

$$\frac{\partial(\rho k)}{\partial t} + \frac{\partial(\rho k u_j)}{\partial x_j} = P_k + G_k - \rho \varepsilon + \frac{\partial}{\partial x_j} \left[\left(\mu + \frac{\mu_t}{\sigma_k} \right) \frac{\partial k}{\partial x_j} \right]$$
 (2.7)

$$\frac{\partial(\rho\varepsilon)}{\partial t} + \frac{\partial(\rho\varepsilon u_j)}{\partial x_j} = C_{1\varepsilon}\frac{\varepsilon}{k}P_k + C_{1\varepsilon}^{(b)}G_k - C_{2\varepsilon}\rho\frac{\varepsilon^2}{k} + \frac{\partial}{\partial x_j}\left[\left(\mu + \frac{\mu_t}{\sigma_{\varepsilon}}\right)\frac{\partial\varepsilon}{\partial x_j}\right]$$
(2.8)

Where P_k is the shear generation term (the rate of turbulent kinetic energy production due to the mean velocity gradient), G_k represents the turbulent kinetic energy contribution due to buoyancy/thermal effects (which must be included if natural convection is present), is the turbulent viscosity (eddy viscosity/turbulent momentum exchange coefficient), and μ_t is the Prandtl number for turbulent kinetic energy (model constant). Advantages: Robust, low computational cost, applicable to fully turbulent flows, and widely used in engineering applications. Disadvantages: Poor accuracy for near-wall, strongly separated, curvature-prone, or rotational flows; requires the use of wall functions or low-Reynolds corrections.

The standard two-equation form of $k - \omega$ is:

$$\frac{\partial(\rho k)}{\partial t} + \frac{\partial(\rho k u_j)}{\partial x_j} = P_k + G_k - \beta^* \rho k \omega + \frac{\partial}{\partial x_j} \left[(\mu + \sigma_k \mu_t) \frac{\partial k}{\partial x_j} \right]$$
(2.9)

$$\frac{\partial(\rho\omega)}{\partial t} + \frac{\partial(\rho\omega u_j)}{\partial x_j} = \gamma \frac{\omega}{k} P_k + G_\omega - \beta \rho \omega^2 + \frac{\partial}{\partial x_j} \left[(\mu + \sigma_\omega \mu_t) \frac{\partial \omega}{\partial x_j} \right]$$
(2.10)

Advantages: Good performance near walls, relatively accurate prediction of the boundary layer and separation onset; no wall function required (can directly solve the viscous sub layer). Disadvantages: Sensitive to the far-field free stream, and requires stricter boundary conditions than $k - \epsilon$ (especially ω).

SST is a hybrid model: it adopts the advantages of $k-\omega$ in the near-wall region and the robustness of $k-\epsilon$ in the freestream region. The Fig. 2.1 shows the $k-\epsilon$ model away from the wall (free stream region) to the $k-\omega$ model close to the wall.

Two mixing functions F_1,F_2 are used to achieve a smooth transition between the inside and outside of the wall; a shear stress limiter is added to the dynamic viscosity model to avoid excessive viscosity (improving the ability to predict separation); and a cross-diffusion term is included in the ω equation to improve numerical stability in the transition region. Common viscosity expressions in SST:

$$\nu_t = \frac{a_1 k}{\max(a_1 \omega, SF_2)} \tag{2.11}$$

where a_1 is a constant (often taken as approximately) and S is a scalar of strain rate. The max term in the denominator limits the excessive growth of eddy viscosity in the strong shear/separation region.

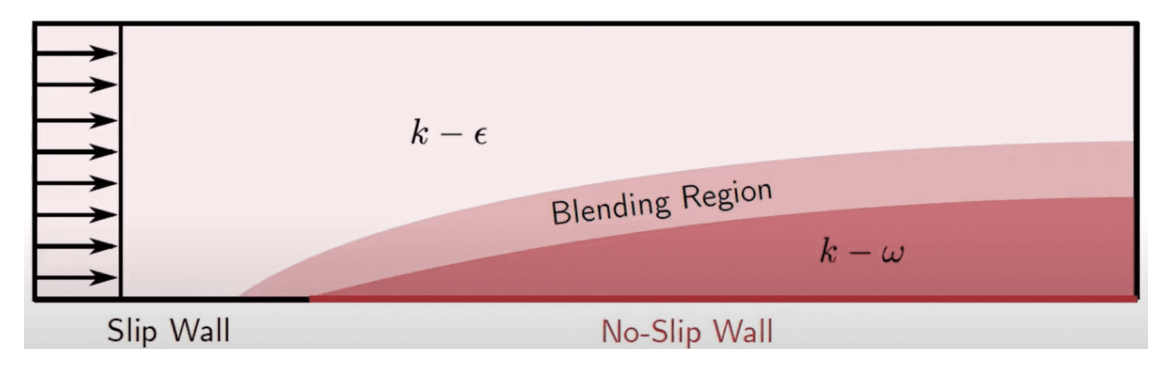


Figure 2.1: $k - \omega$ SST model switches between $k - \epsilon$ and $k - \omega$ turbulence model [7]

The Generalized $k-\omega$ (GEKO) model is based on the $k-\omega$ model but introduces adjustable modeling parameters, allowing users to optimize for different flow types. Through parameterization, it can cover performance from $k-\epsilon$ to $k-\omega$ and SST. Its advantage is greater versatility; there's no need to switch between $k-\epsilon$, $k-\omega$, and SST depending on the operating conditions; GEKO can achieve similar results through parameter adjustments. In terms of adjust ability, users can adjust parameters based on empirical data or experimental results, achieving greater accuracy for specific applications. The model is also more stable and more robust to far-field boundary conditions than the traditional $k-\omega$ model. However, since GEKO was introduced only recently, it requires experience to adjust parameters according to user requirements; otherwise, it degenerates to the standard $k-\omega$ model. The equation form of GEKO is:

$$\frac{\partial(\rho k)}{\partial t} + \frac{\partial(\rho U_j k)}{\partial x_j} = P_k - D_k + \frac{\partial}{\partial x_j} \left[\left(\mu + \frac{\mu_t}{\sigma_k} \right) \frac{\partial k}{\partial x_j} \right]$$
(2.12)

$$\frac{\partial(\rho\omega)}{\partial t} + \frac{\partial(\rho U_j\omega)}{\partial x_j} = C_{\omega 1} F_1 \frac{\omega}{k} P_k - C_{\omega 2} F_2 \rho \omega^2 + \rho F_3 C_D + \frac{\partial}{\partial x_j} \left[\left(\mu + \frac{\mu_t}{\sigma_\omega} \right) \frac{\partial\omega}{\partial x_j} \right]$$
(2.13)

where the usual symbols are:

- ρ : fluid density,
- U_j : velocity component in x_j direction,
- k: turbulent kinetic energy,
- ω : specific dissipation rate,
- μ : molecular viscosity,

- μ_t : turbulent (eddy) viscosity,
- σ_k, σ_ω : turbulent Prandtl-like diffusion coefficients,
- P_k : production of k (commonly $P_k = \tau_{ij} \frac{\partial U_i}{\partial x_j}$ or modeled by $\mu_t S_{ij} S_{ij}$),
- D_k : destruction/dissipation of k (often $D_k = \rho \beta^* k \omega$ in standard forms),
- $C_{\omega 1}, C_{\omega 2}$: model constants,
- F_1, F_2, F_3 : blending / tuning functions used by GEKO (contain adjustable coefficients),
- C_D : additional dissipation or correction term (model-dependent).

2.3.2 Analytical modeling technique

Analytical modeling methods simplify the modeling and calculation of motor temperature rise and heat dissipation based on theoretical formulas from thermodynamics, electromagnetic, and heat transfer. Principle: The motor is abstracted into a thermal resistancecapacitance network and calculations are performed using energy conservation, Fourier's law, and convective heat transfer formulas. Its advantages include intuitive modeling and fast calculations; rapid temperature rise assessments in the early stages of motor design; and ease of integration with control strategies for real-time thermal management. Its limitations include reliance on assumptions (such as uniform materials and simplified geometry), lower accuracy than numerical and CFD simulations; and difficulty in capturing local hot spots and complex cooling circuits. Typical applications include preliminary motor thermal design, real-time thermal management systems, and rapid thermal sensitivity analysis. This paper draws on a thermal modeling technique based on a lumped parameter thermal network (LPTN) [1]. Thermal models based on this approach have been widely used to analyze the thermal performance of electric motors. The LPTN model has even been used to analyze the impact of different cooling methods on the electromagnetic performance of electric vehicle traction motors. Therefore, the LTPN model not only provides a high-fidelity simulation solution but also enables computationally efficient thermal analysis. The LPTN approach is used to calibrate the thermal model for the proposed fuel injection cooling configuration. Simulation results are compared with test results.

2.4 Software Technical Support

The use of software is essential for case studies. An IPM motor was selected, and the corresponding geometric model, material properties, and performance data, including output power, were acquired as the basis for the study. This data was then input into Motor CAD software for electromagnetic and thermal analysis. Based on the motor geometry of motor, 3D modeling was performed using CATIA software. The resulting model was then imported into ANSYS software, such as Space-Clam to set boundary

surfaces and ANSYS FLUENT to create the mesh. Finally, a simulation was performed to verify convergence.

2.4.1 Motor CAD

Motor-CAD is a professional software developed by Motor Design Ltd. specifically for motor design and analysis. It is widely used in the research and development of various motors, such as those in electric vehicle drive systems and industrial motors. In the early stages of design, engineers can use the software to quickly perform multi-physics simulation analysis of motors. Features include electromagnetic analysis, thermal analysis, mechanical analysis, and system integration and optimization. This article focuses on electromagnetic and thermal analysis. In electromagnetic analysis, the effects of three different cooling circuits on the electromagnetic performance and maximum torque of the motor are studied. In thermal analysis, the temperature distribution of the winding, core, magnets, and other components is predicted, and the steady-state and transient thermal performance of the motor is calculated.

2.4.2 CATIA

Developed by Dassault Systèmes of France, CATIA is a world-leading 3D design and engineering software. More than just Computer-Aided Design(CAD) software, it integrates multi-disciplinary capabilities across Computer-Aided Design(CAD), Computer-Aided Design(CAM), and Computer-Aided Engineering(CAE). It is widely used in industries such as aerospace, automotive, shipbuilding, machinery manufacturing, and construction. Based on the geometric structure data of motor, the Mechanical Design module is used to create 3D modeling of each component. Starting with a sketch, the model progresses from points to surfaces, and then to solids. Based on the structure, grooves, holes, and mirroring are used. The motor modeling includes the shaft, rotor lamination, magnet, stator lamination, air gap, winding, and water jacket. Subsequently, the components are imported into the Product module for assembly. First, a fixed constraint is applied to the shaft as an anchor point. Center, distance, and contact constraints are then applied to the relative positions of the components to complete the motor assembly.

2.4.3 ANSYS

ANSYS, developed by ANSYS Inc. in the United States, is a leading global engineering simulation software. It provides engineers and researchers with simulation solutions in fields such as structures, fluid dynamics, electromagnetic, thermal analysis, and multiphysics coupling. The ANSYS suite of software is widely used in industries such as aerospace, automotive, energy, electronics, and civil engineering, helping companies reduce R&D costs, shorten product cycles, and improve performance. In this project, ANSYS SpaceClaim and ANSYS FLUENT, two of the software components, were primarily used. First, the 3D model was saved and imported into ANSYS SpaceClaim. The contact boundaries of each model component were defined and named. For example, the contact surface between the air gap and the rotor lamination had two unique periodic

surfaces. Since the model only had one-eighth of a motor pole, two rotating periodic surfaces were required to simulate the rotation. After defining the surfaces, the model was imported into ANSYS FLUENT. The local mesh size, boundary layer settings, and other features were configured for the component meshes. Finally, the mesh for the volume was generated. After meshing the model, go to the solution module and set the temperature, heat transfer conditions, and motion conditions for the material of each component, boundary layer, and contact surface. After initialization, solve the model and obtain the simulation results for temperature and pressure.

2.5 Overview of cooling strategy

Heat generation in electric vehicle motors is an inevitable physical phenomenon, but effective cooling solutions can effectively safeguard motor efficiency and lifespan. As electric vehicle power continues to increase, liquid cooling and new heat dissipation technologies will become mainstream trends. Intelligent and integrated thermal management systems will also drive further development of the electric vehicle industry. This section will detail motor cooling strategies. Based on recent research, motor cooling strategies include natural, forced air, forced liquid, and phase change cooling [3]. In this article, forced liquid cooling is employed.

2.5.1 Natural Passive Cooling

Natural cooling utilizes natural convection and radiation between the motor surface and the ambient air to dissipate heat, eliminating the need for additional cooling equipment. Its advantages include the simplest structure, lowest cost, and no maintenance. It is typically used in low-power motors and light electric vehicles (such as electric two-wheelers and electric scooters). However, its limitations include limited heat dissipation capacity, making it unsuitable for medium- and high-power motors, and significant temperature fluctuations. The heat transfer rate from fins to the ambient environment [3]. The fin configuration is shown in Fig.2.2.

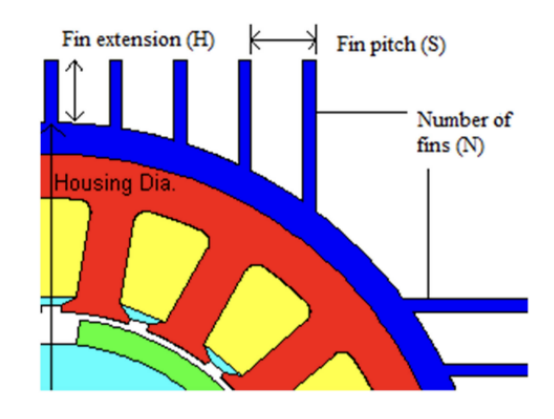


Figure 2.2: Fin configuration geometry [3]

2.5.2 Forced Air

By using a built-in fan or external blower to force air flow into the motor, heat transfer between the motor surface and the air is accelerated. This solution offers advantages in terms of relatively simple structure and significantly improved cooling compared to natural cooling. However, its disadvantages include limited cooling efficiency, which is constrained by the thermal conductivity of air; relatively high noise levels; and reduced heat dissipation at high altitudes or in high-temperature areas. It is commonly used in low- and medium-power electric vehicles, early electric buses, and some commercial vehicles. The ventilation structure of an EFC motor is shown in Fig.2.3.

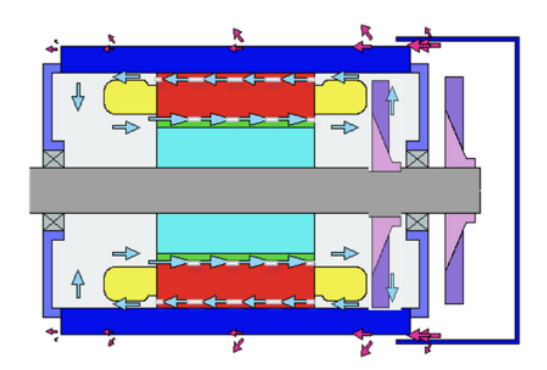


Figure 2.3: Ventilation structure of an EFC motor [3]

2.5.3 Housing water jacket

Annular or spiral cooling channels are installed on the outer wall of the motor housing, through which coolant circulates via a water pump, removing heat. Advantages include a mature and highly reliable system; it dissipates heat from both the motor and controller, forming a unified cooling circuit. However, a disadvantage is the long heat dissipation path, which can still lead to high internal temperature rises in the stator windings and rotor. This system is typically used in mainstream mid- to high-power electric vehicle motors (such as those in passenger cars and commercial vehicles). The forced-liquid cooling model is shown in Fig.2.4.

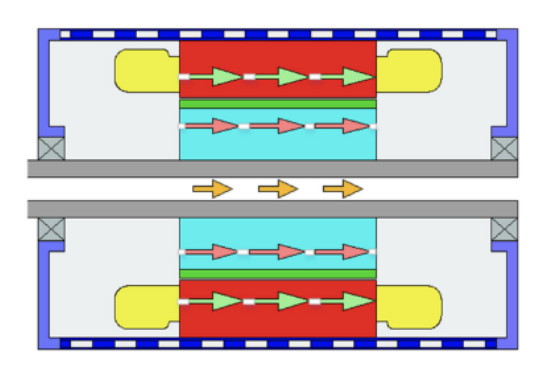


Figure 2.4: Forced-liquid cooling model [3]

2.5.4 Stator cooling

Cooling channels are embedded directly in the stator windings or core, allowing the coolant to directly reach the primary heat source. This approach offers advantages such as efficient heat dissipation, rapidly reducing winding and stator temperatures, and increasing motor power density. However, its disadvantages include a complex structure, demanding machining processes, and reliability influenced by sealing and fluid path design. This approach is commonly used in high-performance electric vehicles and racing motors. The Wet stator cooling system is shown in Fig.2.5.

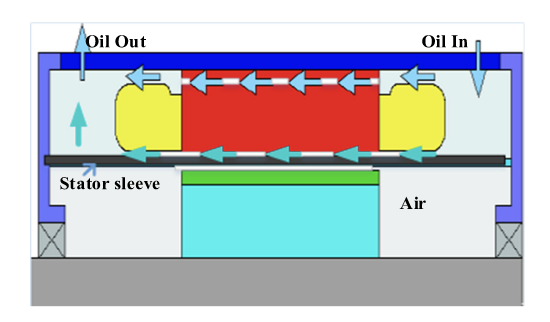


Figure 2.5: Wet stator cooling system [3]

2.5.5 Rotor cooling

Designing cooling channels within the rotor or using oil jet cooling introduces a cooling medium directly into the rotor area, removing heat from the permanent magnets or core. This method effectively prevents permanent magnet demagnetization and ensures reliable high-power operation of the motor. However, its disadvantages include the complexity of sealing and fluid transmission design, as well as high manufacturing and maintenance costs. It is commonly used in high-speed, high-power permanent magnet synchronous

motors. Rotor cooling can be achieved through internal cooling channels, oil jet cooling, and hollow shaft cooling. This article focuses on internal cooling channels and hollow shaft cooling.

- Internal Cooling Channels: Coolant channels are machined close to the rotor lamination or magnets and introduced through a rotating joint or hollow shaft. The advantage of this method is that it allows direct cooling of the heat source and precise temperature control. The disadvantage is that the manufacturing process is complex and requires rotational reliability.
- Oil Jet Cooling: Cooling oil is sprayed onto the rotor surface or winding ends via
 an oil pump, creating an oil film that lubricates and cools the rotor. The advantage
 is that it combines lubrication and cooling functions, with high cooling efficiency.
 The disadvantage is the need for an additional oil system, resulting in higher oil
 aging and maintenance costs.
- Hollow Shaft Cooling: A hollow channel is designed in the center of the rotor shaft to channel coolant through the shaft into the rotor and then out. The advantage is a relatively compact structure that can be integrated with the stator water cooling system. The disadvantage is the design complexity and the need to ensure the reliability of the rotating seal.

The Indirect rotor cooling scheme is shown in Fig.2.6.

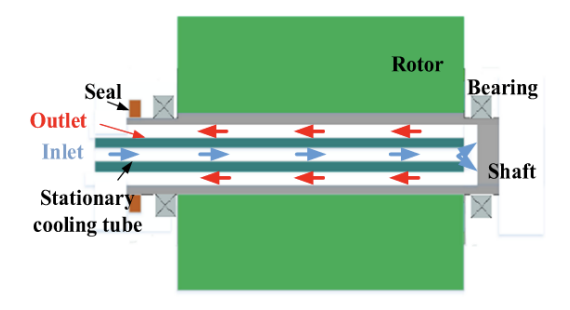


Figure 2.6: Indirect rotor cooling scheme [3]

2.5.6 Phase change

Phase change material (PCM) or phase change coolant are used to control motor temperature by absorbing latent heat during operation. This method offers the advantage of efficient heat absorption, which can quickly suppress rapid temperature increases and is suitable for peak operating conditions. However, its disadvantage is that heat dissipation relies on the thermal storage capacity of the PCM, resulting in limited sustained cooling capacity and requiring integration with other cooling methods. It is typically used in short-term, high-load scenarios, such as racing cars and heavy-duty electric vehicles. The Primary components of a phase change cooling loop is shown in Fig.2.7.

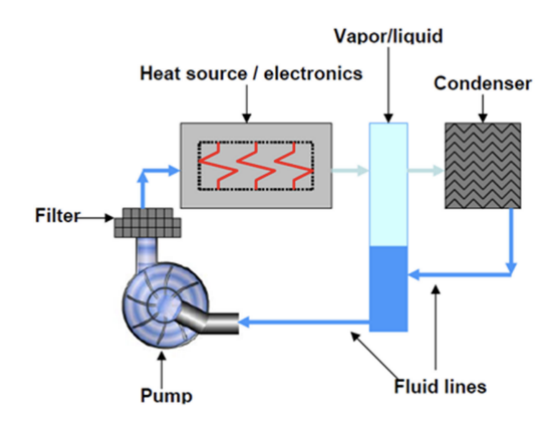


Figure 2.7: Primary components of a phase change cooling loop [3]

Chapter 3

Methodology

3.1 Design of cooling strategies

This study analyzed a 47 kW IPM motor for traction applications. This motor features an 8-pole configuration and a maximum speed of 16,000 rpm. The rotor has an outer diameter of 175 mm, an effective lamination length of 105 mm, and a hollow shaft with an inner diameter of 20 mm as the cooling channel. Three oil cooling strategies were investigated to evaluate their cooling performance. These strategies are:

- a) Case.1: Rotor shaft cooling
- b) Case.2: Rotor shaft and rotor lamination cooling
- c) Case.3: Rotor shaft with direct oil-cooled magnet cooling

Next, the oil circuit is described. The radial and axial cross view of motor are shown in Fig.3.1&3.2. In a), the coolant flows axially along the hollow shaft, with equal flow rates through the inlet and outlet of the hollow shaft. In b), a cooling channel is machined above the magnet position within the rotor lamination. The oil enters from one end of the hollow shaft, passes through the end cap, and flows into the cooling channel in the rotor lamination, thereby allowing direct contact between the cooling oil and the rotor lamination before eventually exiting through the channel outlet. In c), the oil also enters from one end of the hollow shaft. Similar to case b), it flows through the end cap into the cooling channel of the rotor lamination. However, unlike b), case c) utilizes the gap between the rotor lamination and the magnet as the cooling channel, rather than machining an additional channel within the lamination. This design enables the cooling oil to cover the magnet, ensuring direct contact between the oil and the magnet while simultaneously enhancing the direct contact between the oil and the rotor lamination.

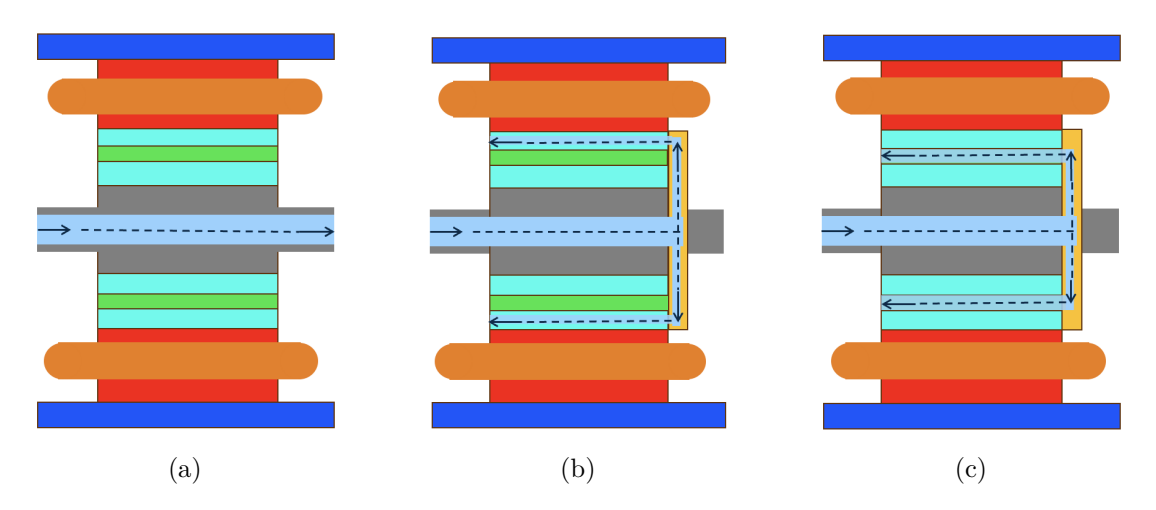


Figure 3.1: Axial cross view of cooling strategies: (a) Rotor shaft cooling, (b) Rotor shaft and rotor lamination cooling, and (c) Rotor shaft with direct oil-cooled magnet cooling. Arrows denote the fluid flow.

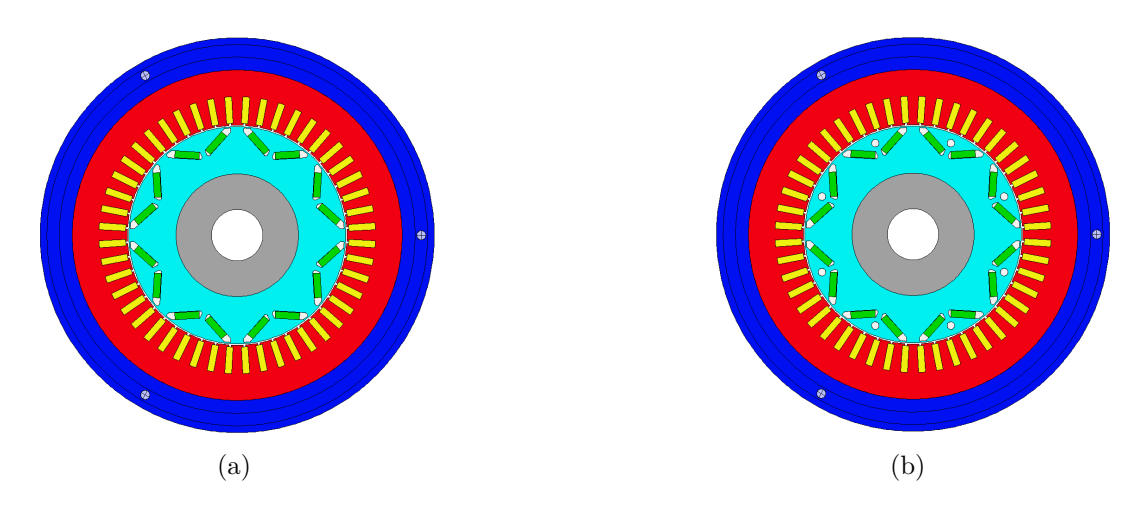


Figure 3.2: Radial cross view of cooling strategies: (a)case.1&3(b)case.2

3.1.1 Case 1

The design of case.1 combines housing water jacket cooling with hollow shaft coolant dissipation. Indirect cooling of the stator is achieved through the water jacket, while direct cooling of the rotor is realized by introducing coolant into the shaft. Coolant flows through the water jacket and shaft cavity, removing heat generated by the motor and transferring it to an external heat sink.

The operating process is as follows: coolant enters the water jacket in the motor housing via a water pump and flows around the stator. Heat generated by the stator windings and core is transferred to the coolant through the housing. Heat from the rotor is partially conducted through the air gap to the stator and removed, while another portion is transferred through the shaft to the shaft end cavity, where it is absorbed by the coolant. Finally, the coolant flows to an external heat sink, releasing the heat, completing the heat exchange cycle.

The technical advantages are maturity and reliability: housing water jacket cooling is widely used in motors and the process is mature. Good integrity: It simultaneously dissipates heat from both the stator and rotor, mitigating localized hot spots. High scalability: The water jacket design allows for adjustable channel cross-sections and flow rates based on power requirements. The shortcomings of the technology are: the heat dissipation efficiency inside the stator winding (especially the ends) is limited, and local hot spots may exist; rotor cooling is still mainly based on indirect heat dissipation, which is not as effective as direct oil cooling. The geometric model of case.1 shows in Fig.3.3:

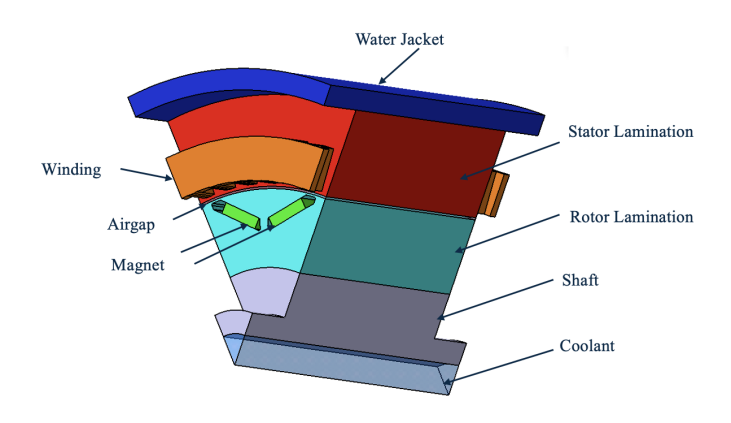


Figure 3.3: 3D geometric model of case.1

3.1.2 Case 2

Case 2 shares a similar cooling circuit design to Case 1. This cooling solution also utilizes a dual cooling system within the motor. This approach is suitable for handling high winding heat and ensuring the life of motor insulation. The internal shaft cooling channels allow coolant to flow through hollow channels within the shaft, then be directed through the end caps before returning. This design effectively cools the rotor and bearing areas, preventing overheating and demagnetization of the rotor magnets. The coolant circulation path is as follows: the coolant first flows from the center of the shaft, flows through the interior of the rotor, then returns to the end caps, exits the cooling channels, and ultimately returns to the cooling system. This circuit ensures efficient convective heat transfer and a uniform temperature distribution within the motor. The key difference lies in the cooling channels. Compared to Case 1, Case 2 includes cooling channels leading to the rotor lamination, increasing the cooling area, and shortening the distance to core heat-generating components. This design offers the following advantages: efficient heat dissipation, combining water jacket and internal shaft cooling to cool both the stator and rotor simultaneously; preventing demagnetization by directly cooling the rotor magnets,

reducing the risk of high temperatures; a compact design, with cooling channels integrated into the shaft and end caps, resulting in a compact structure that does not significantly increase the overall dimensions; and improved temperature uniformity, which reduces hot spots within the motor and enhances motor performance stability. The geometric model of case. 2 shows in Fig. 3.4:

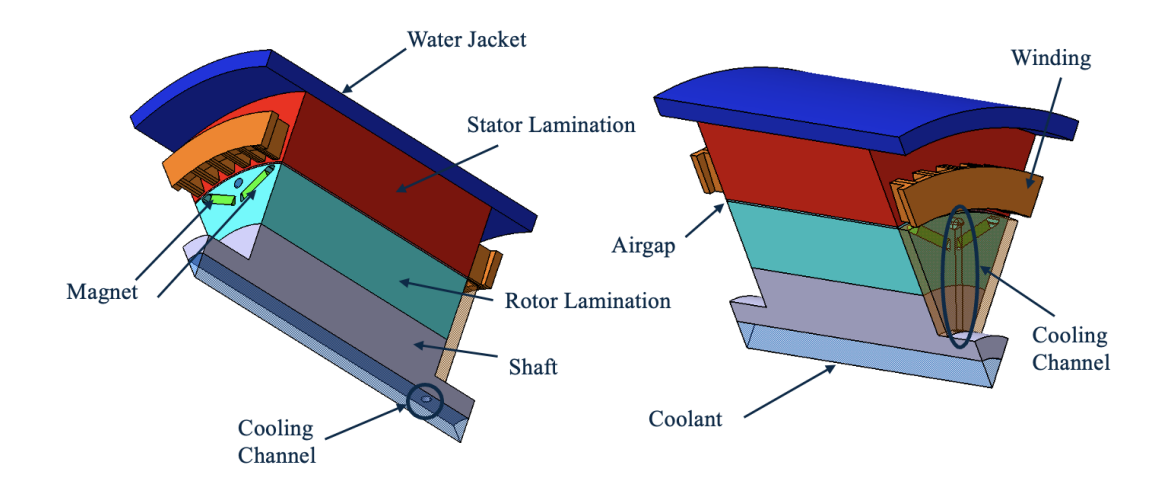


Figure 3.4: 3D geometric model of case.2

3.1.3 Case 3

Compared to the cooling circuit design of Case 2, its cooling path does not directly cover the magnet area, resulting in a certain temperature gradient. Case 3 improves upon this: the coolant flows through cooling channels located at the magnet location. The cooling channel location is optimized, extending the coolant channel from simply inside the rotor shaft to cover the magnet area. Direct cooling of the magnets is more advantageous for heat dissipation, as it accelerates the cooling rate and reduces the local temperature rise of the magnets. The coolant enters through the center of the shaft, circulates inside the rotor, and returns at the end cap into the cooling channels surrounding the magnet region. It covers the magnets and absorbs their heat before flowing out through the outlet and back to the cooling system. This design allows for more direct contact between the coolant and the magnets, reducing the heat transfer path and improving cooling efficiency. The advantages of Case 3 are primarily reflected in the following aspects: significantly enhanced magnet cooling capacity, and direct coolant coverage of the magnets, eliminating the risk of demagnetization due to excessive temperature rise. More uniform temperature distribution and a more balanced temperature field within the rotor reduce local overheating and improve motor stability. This increases power density potential, lowers magnet temperature, and enables the motor to operate at higher current densities, thereby increasing power output. This enhances system reliability by directly cooling the magnets and the area surrounding the bearings, helping to extend motor life and reduce failure rates. The geometric model of case.3 shows in Fig.3.5:

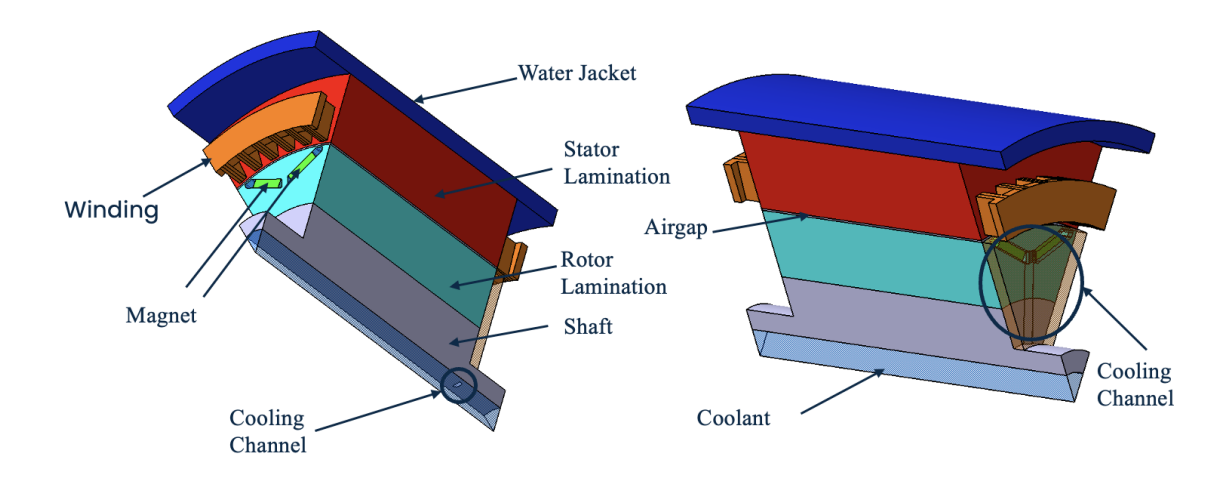


Figure 3.5: 3D geometric model of case.3

3.2 Set-up of model

First, use SpaceClaim to group the boundary surfaces of the geometric model, such as housing walls, roto lamination walls, and periodic rotation surfaces. Then, set the mesh size and local mesh values. For example, for areas requiring high mesh fineness, set the airgap size to 0.5mm, the fluid to 1mm, the less critical winding and lamination to 2mm, and the rest of the overall settings to a minimum of 1mm and a maximum of 3mm. After importing, generate the fluid domain and check whether the model is closed. Set the number of boundary layers in the fluid domain to 5 to meet the y+value requirements. Finally, automatically generate the volume mesh and check the mesh quality. For example, in Case 2, the skewness of 0.76 is considered good, and the orthogonal quality of 0.21 is also considered good.

After meshing is complete, set the boundary conditions. First, select the appropriate physical model based on your research objectives. In the Model tab, enable the appropriate equations for flow and heat transfer. Since heat transfer is involved, the energy equations must be enabled. The cooling channels in this research model involve the flow of cooling oil, which involves a fluid domain, so the GEKO model is used as the turbulence model.

Next, define the required fluid or solid materials in Materials. Directly use built-in air material of ANSYS FLUENT as the material for the air gap of motor. Customize the material by entering parameters such as density, viscosity, thermal conductivity, and specific heat capacity to set the cooling oil material, the housing material, the magnet material, and the shaft material, as shown in the Table 3.1. In the Cell Zone Conditions

module, set the materials and thermal sources for the fluid and solid components, such as the heat transfer coefficient of magnet(dividing the heat loss of magnet 66.29W by its volume yields a final value of $823134kg/(m^2/s)$)). Next, set boundary conditions in the Boundary Conditions module. Set the coolant inlet flow rate to 4.261m/s (calculated by dividing 10L/min by the inlet area). Walls are no-slip boundaries by default. For example, set the convection heat transfer coefficient of $1873.044W/(m^2/K)$ for the housing wall. Also, set periodic rotating boundary conditions for the periodically rotating boundary surface defined previously.

After all model parameters are set, initialization is required. Fluent offers both Standard Initialization and Hybrid Initialization. The Hybrid method automatically generates a reasonable initial flow field and is suitable for most problems. For transient calculations, the steady-state solution can be used as the initial condition to reduce convergence time. In this article, Hybrid Initialization is selected. After initialization is complete, you can proceed to the Run Calculation stage. Set the number of iterations and the time step to 20, then start the calculation. During the calculation, you can observe the residual curve in real time and monitor the pressure drop and temperature distribution at the inlet and outlet of the cooling channel to ensure that they gradually stabilize with the iteration process. Only when both the residual and the monitored variables are stable can the calculation results be considered converged.

Finally, the convergence results need to be verified. Convergence depends not only on the residual curve but also on checking whether mass conservation is satisfied, that is, whether the inlet and outlet flow rates are balanced. It is also necessary to evaluate whether the velocity and temperature field distributions are reasonable. This completes the Fluent Solution process. Next, you can use built-in post-processing tools of ANSYS FLUENT to generate graphical results such as the pressure and temperature fields.

Material	Density (kg/m^3)	Specific heat $(J/(kg.k))$	Conductivity $(w/(m.k))$
Copper	8933	385	anisotropy
N42SH	7500	460	7.6
NO 18-1160	7650	460	27
Stahl 37	7800	450	25
ATF134	828.6	2160	0.136
Epoxy	2100	1000	1.5

Table 3.1: The table of all the materials

3.3 Equivalence of components

Electric motors, like permanent magnet synchronous motors and induction motors, often have a uniform distribution of forces around the circumference. For example, if a motor has eight pole pairs and eight slots, the geometry and flow within the motor repeat at regular intervals. Therefore, to reduce computational effort in later stages of the study, a single sector of the motor can be used as the computational domain to represent the entirety. In this paper, one-eighth of the motor was selected as the research object.

Therefore, in the later stages of the model simulation, periodic boundary conditions must be set for the model. On the two side slices, the flow is not enclosed by a solid, so walls cannot be set. Instead, the adjacent sectors should be connected. This requires periodic boundary conditions, which automatically replicate or mirror the flow field on one side of the slice to simulate a complete circumferential distribution. The periodic boundary surfaces show in Fig.3.6. Specifically, rotating periodic boundaries are suitable for symmetric geometries like motors. In ANSYS FLUENT, the flow field remains the same at the same angle when two slices are 45° apart. This allows the fluid flow to be contained within the 1/8 model, effectively joining eight small sectors to form a complete motor. The advantages are that the amount of calculation is greatly reduced, and the physical correctness is maintained, that is, the flow field is guaranteed to be continuous in the circumferential direction. It can also reflect the geometric symmetry of the motor and is more in line with the actual working conditions.



Figure 3.6: Periodic boundary conditions: (a) Rotational periodic boundary surface of one-eighth motor.1(b)Rotational periodic boundary surface of one-eighth motor.2

3.3.1 Equivalence of the Winding

The CFD simulation provides an effective method for analyzing temperature distribution in electric motors, eliminating the need for physical experiments while ensuring accuracy and saving costs. However, accurate results depend on the accuracy of the thermal model. Within the motor stator, the windings are the primary heat source. Due to the stacked arrangement of copper conductors and insulation, the windings exhibit anisotropic thermal conductivity. The low thermal conductivity of the insulation hinders radial heat transfer, significantly reducing the radial thermal conductivity of the windings. Furthermore, the complex composite structure of winding, consisting of multiple coils with thin insulation and delicate geometry, presents significant meshing challenges and imposes high computational requirements. To simplify the model and reduce computational complexity, the windings can be treated as a single entity with anisotropic behavior, consisting of copper and non-copper materials, namely insulation. All non-copper materials can be treated as equivalent homogeneous media, and their effective thermal conductivity is determined

by taking the area-weighted average of the thermal conductivities of all components.

Next, we will conduct a more in-depth calculation and analysis of the equivalent thermal conductivity of winding. A two-dimensional winding model was viewed in Motor CAD. The winding consists of n layers of coils, as shown in Fig.3.7. The yellow portion represents copper wire, while the green gaps between the windings are filled with equivalent insulation. Copper strips are connected in parallel with the insulation in the axial direction and in series with the insulation in the radial direction, and the equivalent thermal conductivity is calculated using a thermal resistance layout. The thermal resistance layout shows in Fig.3.8. In ANSYS FLUENT, a heat flux boundary condition was applied to the outer surface of the winding to add a heat source.

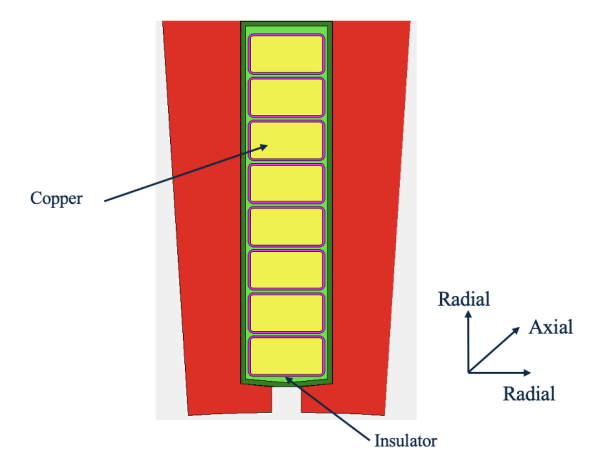


Figure 3.7: Winding cross section

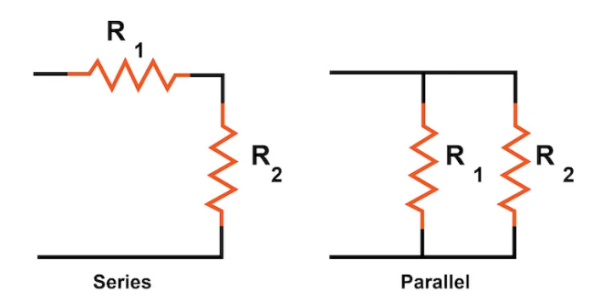


Figure 3.8: Thermal resistant layout

Anisotropic thermal conductivity coefficient:

$$K_{ax} = F_f \times K_{Cu} + (1 - F_f) \times K_{ins}$$
(3.1)

$$K_{rad} = \frac{K_{Cu} \times K_{ins}}{F_f \times K_{ins} + (1 - F_f) \times K_{Cu}}$$
(3.2)

Where K_{ax} is Axial thermal conductivity of rotor winding, K_{rad} is Radial thermal conductivity of rotor winding, F_f is Filling Factor, K_{Cu} is Thermal conductivity of copper, K_{ins} is Thermal conductivity of insulator.

Equivalent thermal conductivity is calculated by the thermal resistant:

$$R = \frac{L}{KA} \tag{3.3}$$

According to equations 3.1&3.2, the thermal conductivity of copper is $401W/(m*^{\circ}C)$, the thermal conductivity of the insulation is $0.21W/(m*^{\circ}C)$, and the fill factor for all configurations is 0.856. Therefore, the equivalent axial thermal conductivity is calculated to be $343.286W/(m*^{\circ}C)$, and the equivalent radial thermal conductivity is calculated to be $1.454W/(m*^{\circ}C)$. The calculated results show that the radial thermal conductivity is much lower than the axial thermal conductivity, once again reflecting the anisotropy of the winding.

During the pole winding process, the local principal axis of the anisotropic thermal conductivity will change relative to the direction of the global coordinate system. This change in direction mainly occurs in the winding end area and is constrained by the geometric shape of the winding. In order to simplify the calculation, the method of curvilinear coordinate system was adopted. Specifically, the winding field is regarded as an equivalent fluid domain, and the inlet and outlet boundaries are set for the axial cross-section, bottom and top of the winding respectively. The axial cross-section is converted from the y-axis inflow direction to the x-axis outflow direction, and the bottom of the winding flows from the radial inflow to the top outflow while maintaining the z-axis direction. In each grid cell, the local velocity direction is specified as its principal axis, and the corresponding thermal conductivity value is set as the axial thermal conductivity component. The curvilinear coordinate system for winding shows in Fig.3.9:

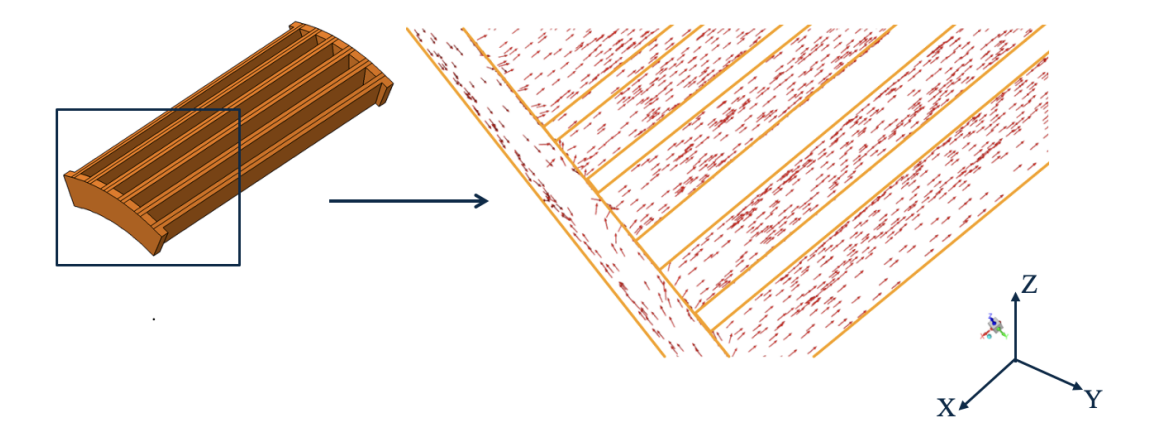


Figure 3.9: Curvilinear coordinate system for winding

3.3.2 Equivalence of the Rotor and Air-gap

The air gap between the Rotor and Stator, as well as the air gap between the Magnet and Rotor, were modeled, and convection was simulated by defining air properties in ANSYS. In actual modeling, in order to reduce the amount of calculation for the air gap mesh, the air gap was not modeled in the CATIA modeling, which the two planes were in contact. After importing into ANSYS FLUENT, when setting up the Solution, the air gap thickness was set to 0.2mm and the air thermal conductivity properties were set to be equivalent to the air convection. For the equivalence of the bonding surface between the magnet and the rotor, the wall thickness was set to 0.1mm and the thermal conductivity properties of the glue material were set to simulate conduction. On the surface of the rotor lamination, the frozen rotor method was used to convert the transient rotation into a steady-state problem, and a rotation speed of 16,000 rpm around the x-axis was imposed on the rotor wall to simulate the rotation of the motor. The geometric model of the equivalence of rotor and air-gap shows in Fig.3.10:

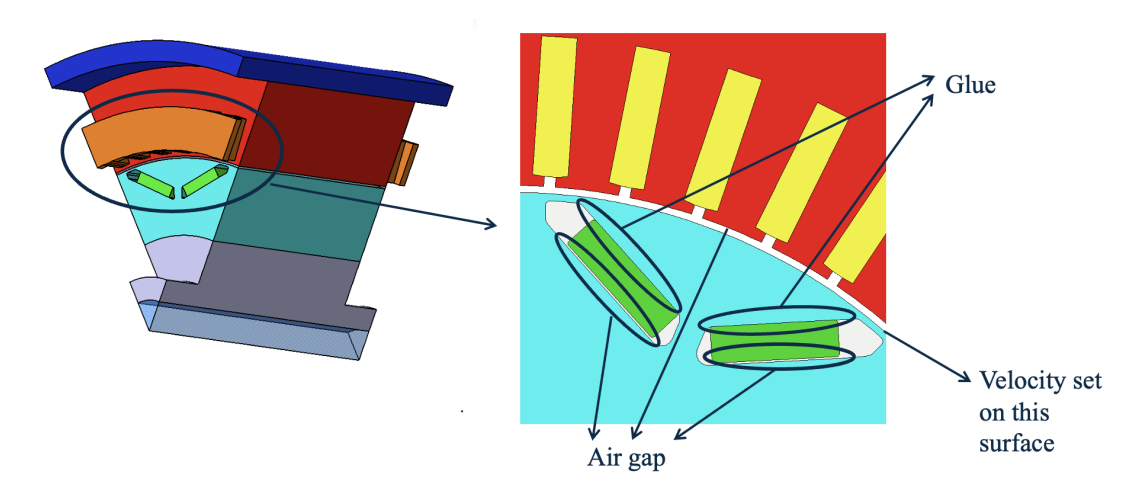


Figure 3.10: Equivalence of the Rotor and Air-gap

3.3.3 Equivalence of the Stator Water Jacket

Since the water jacket has a spiral cooling channel inside, the contact area between the water jacket and the stator lamination is different between the one-eighth motor model and the complete motor model. In order to equivalent the cooling area of the complete water jacket and set it in ANSYS FLUENT, it is necessary to use equations 3.5&3.6 to calculate the equivalent heat transfer coefficient, where the completed motor surface area of housing wall is $0.051m^2$, the Equivalent motor surface area of housing wall is $0.01m^2$, and the Completed motor heat transfer coefficient is $2952W/(m *^{\circ} C)$. Then, in the solution setting of ANSYS FLUENT, fill in the calculated equivalent heat coefficient of $1873.044W/(m *^{\circ} C)$ for the housing wall. The position of housing wall shows in Fig.3.11.

The calculation formula for the heat transfer coefficient is as follows:

$$Q = A_c \times h_c \times \Delta T \tag{3.4}$$

$$h_e \times A_e = A_c \times h_c \times \frac{1}{8} \tag{3.5}$$

$$h_e = \frac{A_c \times h_c}{A_e} \times \frac{1}{8} \tag{3.6}$$

where the usual symbols are:

- Q: Heat
- A_c : Completed motor surface area of housing wall
- h_c : Completed motor heat transfer coefficient
- A_e : Equivalent motor surface area of housing wall
- h_e : Equivalent motor heat transfer coefficient
- ΔT : The temperature difference

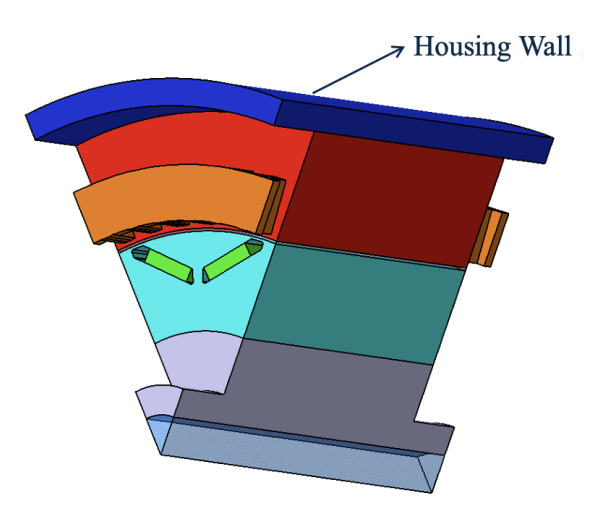


Figure 3.11: Equivalence of the housing wall

3.4 Selection of operating point

The operating point of a motor refers to the intersection of a characteristic of motor curves—encompassing its torque, rotational speed, and losses. The operating point determines the distribution and magnitude of losses; these losses serve as heat sources, which in turn dictate the temperature rise and service life of motor. Under different

operating points (which is, under varying rotational speeds, torques, currents, and frequencies), losses such as iron loss, rotor and stator back loss, magnetic loss, and copper loss (as shown in the Fig.3.12-3.17) change with factors like rotational speed and current. This results in distinct thermal responses, including steady-state temperature rise and transient behavior. Therefore, thermal management must be based on target operating points, covering the design of cooling systems, selection of insulation classes, and definition of continuous or short-term power ratings as well as derating strategies. The selection of operating points is a critical issue in motor thermal management design. When a motor operates under different rotational speeds and torques, its loss level changes significantly; all these losses are eventually converted into heat, leading to an increase in the motor's internal temperature. The core task of thermal management is to ensure that the motor's temperature rise does not exceed the allowable limits of its materials, insulation, and magnets under any operating condition. To achieve this goal, this study selects the operating point with a maximum rotational speed of 16,000rpm and a maximum loss of 2,781W for research.

First, selecting the operating point with maximum loss typically represents the most adverse operating condition for the motor. At this point, various losses—such as copper loss, iron loss, and total thermal loss—may accumulate to the highest level, causing the motor to generate the most severe heat. If the motor's temperature can be maintained within a safe range under this condition, the motor will undoubtedly operate stably under more favorable conditions at other operating points with lower losses. This operating point defines the motor's cooling capacity requirements and safety boundaries.

Second, from the perspective of cooling system design, the capacity of cooling devices (such as water-cooled jackets and oil cooling systems) must be bench marked against the maximum loss point. If the cooling system cannot cope with this operating condition, the motor will overheat during heavy-load or high-speed operation, which in turn leads to insulation aging, permanent magnet demagnetization, or even component failure. Therefore, only by verifying the reliability of the cooling system at the maximum loss point can the safe operation of the entire motor under all operating conditions be guaranteed.

Additionally, researching the maximum loss operating point is equally important for determining the motor's rated performance. The motor's rated torque and rated power are constrained by thermal limits. The motor's capacity for sustained long-term power output is determined by whether or not its temperature rise exceeds the limit under maximum loss conditions. If the temperature fails to meet requirements under the most adverse thermal conditions, the rated values must be reduced or the cooling strategy enhanced.

Finally, from the perspective of service life and reliability, the aging rate of the motor's insulation materials and the risk of demagnetization are closely related to temperature. The maximum loss point typically corresponds to the operating condition where the hotspot temperature is the highest. Without sufficient research on this point, it is difficult to predict the motor's long-term operational life. In conclusion, selecting the operating point with maximum loss as the research object is both reasonable and critical.

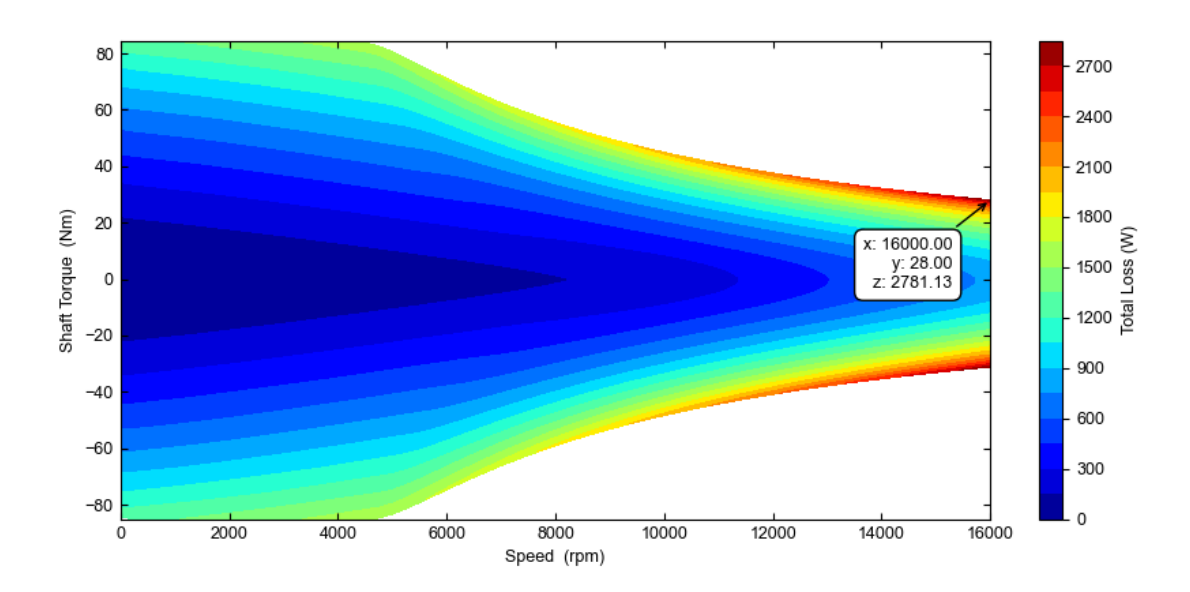


Figure 3.12: The total loss map

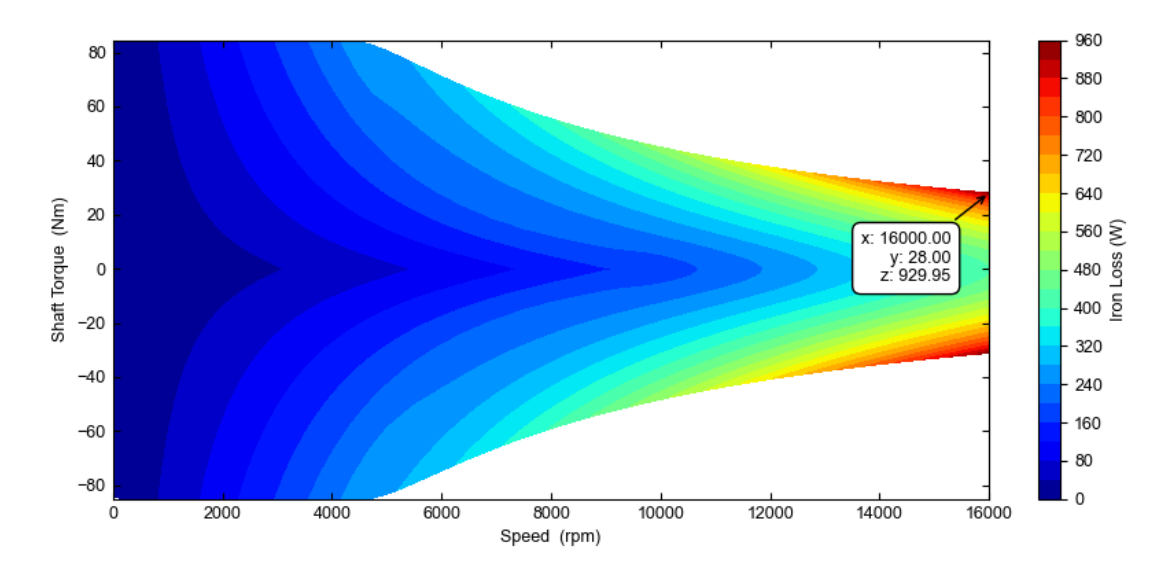


Figure 3.13: The iron loss map

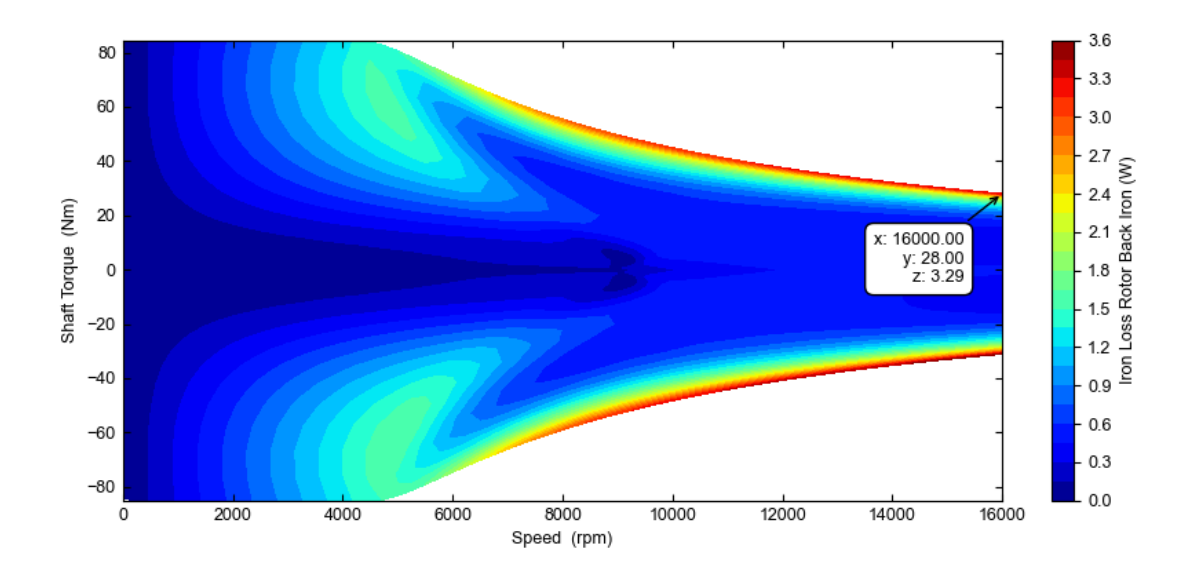


Figure 3.14: The rotor back iron loss map

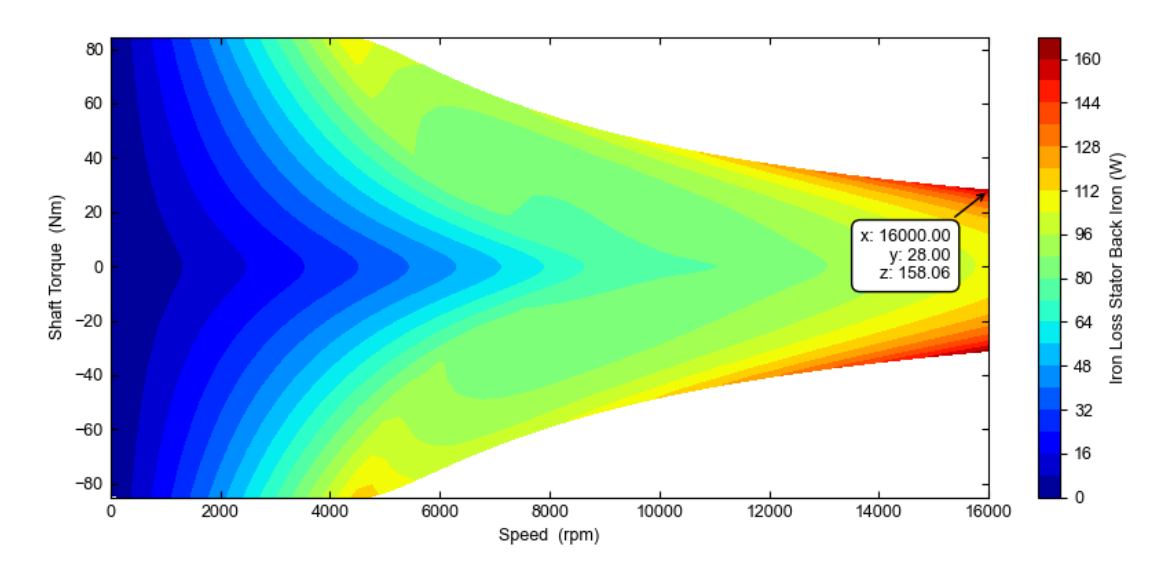


Figure 3.15: The stator back iron loss map

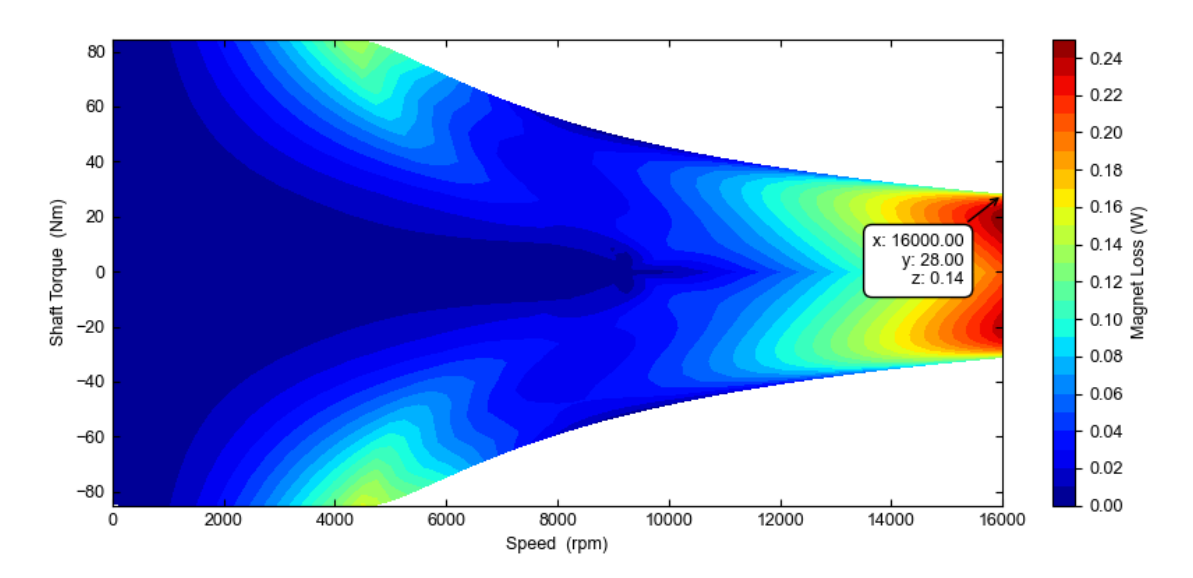


Figure 3.16: The magnet loss map

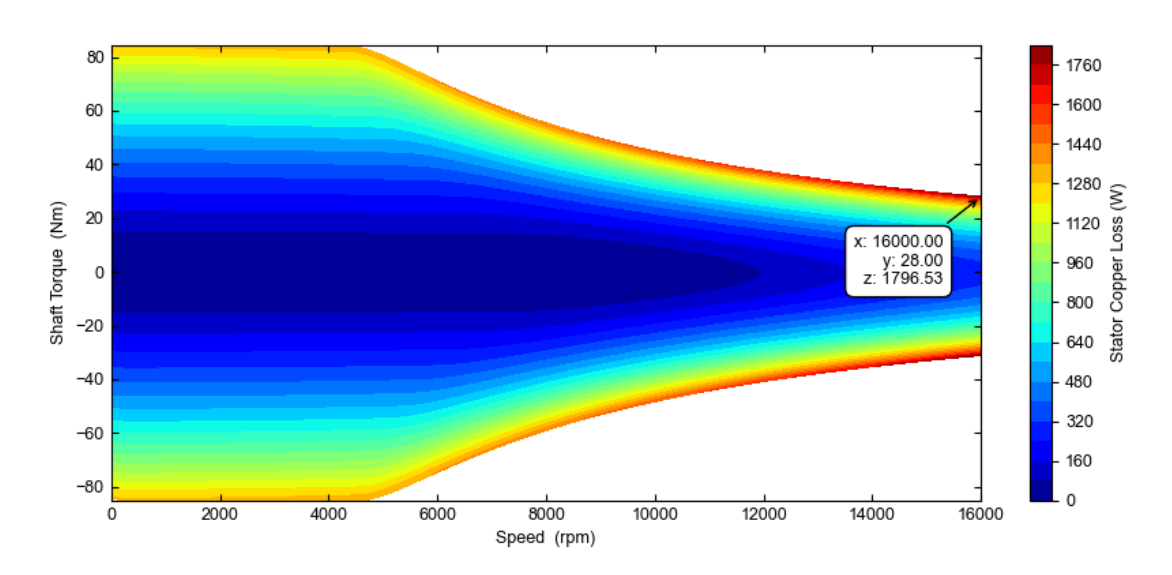


Figure 3.17: The copper loss map

Chapter 4

Results

4.1 Convergence of the model

Residual plot is a key indicator of simulation convergence. A decreasing residual curve and plateauing with iteration number indicate convergence and reliable results. This paper analyzes the residual results of three different motor cooling cases using Fluent simulations, exploring the convergence characteristics and simulation effectiveness of each case. In Fluent simulations, residuals represent the error in solving governing equations (such as the continuity equation, momentum equation, energy equation, and turbulence model equations). The downward trend and final plateau of the residual curve directly reflect the convergence of the numerical calculation: the more significant the curve decreases and the lower the final residual level, the more fully the equations are solved and the more reliable the simulation results. The residual plot is shown in the Fig.4.1.

For the first residual plot a), the number of iterations reaches 1600, and the vertical axis shows the scaled residuals on a logarithmic scale. The residuals of various physical quantities exhibit the following characteristics: For velocity field and continuity, the residuals for x-velocity, y-velocity, and z-velocity (three-dimensional velocity components), as well as the continuity equation, rapidly drop below 10^{-9} after approximately 200 iterations and remain stable for a long time. For energy and turbulence model, the residual for the energy equation gradually decreases to the order of 10^{-8} . The residuals for k and omega stabilize within the range of 10^{-7} (sim 10^{-8}). The residual for continuity ultimately stabilizes around 10^{-7} . The low magnitude of the residuals and the long iteration count of this case demonstrate the extremely high convergence accuracy of its flow and thermal field calculations, indicating that the mathematical equations for fluid flow and heat transfer under this cooling cases are fully solved, and the simulation results are highly reliable. The second residual graph b) shows the following residuals for various quantities after 250 iterations: For continuity and velocity fields, the residual for continuity gradually decreases from its initial value to the order of 10^{-6} ; for x-velocity, y-velocity, and z-velocity, the residuals fall to the range of 10^{-9} (sim 10^{-10}) after 250 iterations; for the energy and turbulence model, the residual for energy decreases to approximately 10^{-10} ; the residual for k ultimately stabilizes at the order of 10^{-8} , and the residual for omega is approximately 10⁻⁸. Compared to Case 1, Case 2 converges significantly faster (reducing the number of iterations by approximately 80%), but the final residuals for quantities like continuity are slightly higher. This demonstrates that the flow and heat transfer processes of this cooling case converged effectively in numerical calculations. While its accuracy was slightly lower than that of Case 1, it fully met the convergence requirements for engineering simulations and supported subsequent cooling performance analysis. Corresponding to the third residual plot c), the number of iterations was 500, and the residual curve characteristics are as follows: Continuity and velocity field: The continuity residual decreased to the order of 10^{-9} ; the x-velocity, y-velocity, and z-velocity residuals stabilized below 10^{-10} after 300 iterations; Energy and turbulence model: The energy residual decreased to the range of 10^{-10} ; the k residual stabilized in the late iterations (to the order of 10^{-7}), and the omega residual ultimately reached approximately 10^{-9} . The number of iterations required for convergence and the residual accuracy of this case lie between Case 1 and Case 2. The k residual is relatively high, likely due to the turbulence intensity distribution characteristics of this solution. However, effective convergence is achieved overall, demonstrating a typical balance between convergence speed and accuracy.

The temperature curve is shown in the Fig.4.2. For Case 1, the winding is the hottest component in this solution. The curve rises rapidly in the early iterations before leveling off, indicating that the winding is the primary heat source and requiring focused optimization of its cooling design. The stator-lamination solution converges quickly and exhibits good thermal stability. The maximum temperature curves of the magnet and rotor-lamination systems almost overlap, demonstrating highly uniform heat distribution on the rotor side and balanced thermal management of the rotor. After approximately 200 iterations, the temperatures of all components in this solution are fully stable, demonstrating strong simulation convergence and verifying the reliability of the heat transfer model. However, the winding temperature is still relatively high. For Case 2, similar to Case 1, the highest temperature component in the motor is still the winding, reflecting the heat load level of the primary heat source within the motor. The curve quickly stabilizes during the iterations, indicating that the cooling medium effectively removes heat and that the heat exchange process is rapidly balanced. The temperatures of the rotor-lamination and magnet systems are relatively low, demonstrating that the heat dissipation design is effective in thermal management. The solution fully converged within 250 iterations, with clear temperature stratification among components. For Case 3, similar to Case 2, the highest motor temperature component remains the Wingding. The curve quickly stabilizes during iterations, demonstrating that the cooling medium effectively removes heat and that the heat exchange process is rapidly balancing. The rotor-lamination and magnet solutions achieve the lowest temperatures of the three solutions, demonstrating that their heat dissipation design provides the best thermal management results. This solution fully converged after 500 iterations. Although the number of iterations was slightly higher than that of Case 2, the lower temperatures and more uniform heat distribution demonstrate that it offers both balanced and reliable thermal management.

The pressure curve is shown in the Fig.4.3. For Case 1, the pressure curve converges completely smoothly after approximately 200 iterations, demonstrating excellent convergence of the pressure field calculation. For Case 2, the pressure curve converges

quickly after approximately 50 iterations, the fastest convergence of the three cases and demonstrating the high efficiency and stability of the pressure field calculation. For Case 3, the convergence becomes stable after approximately 100 iterations, with convergence efficiency between Cases 1 and 2.

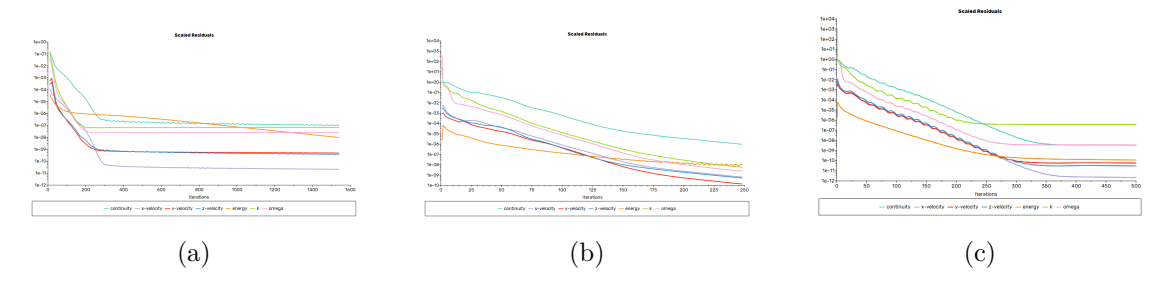


Figure 4.1: The plot of residual of cooling strategies: (a) Rotor shaft cooling, (b) Rotor shaft and rotor lamination cooling, and (c) Rotor shaft with direct oil-cooled magnet cooling.

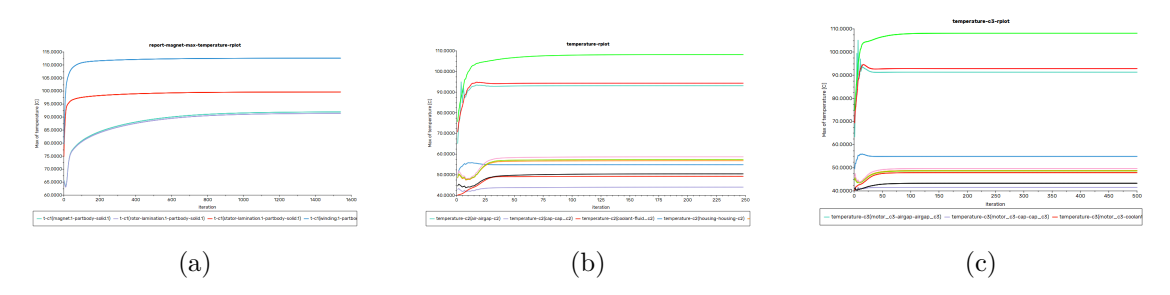


Figure 4.2: The plot of max temperature of cooling strategies: (a) Rotor shaft cooling, (b) Rotor shaft and rotor lamination cooling, and (c) Rotor shaft with direct oil-cooled magnet cooling

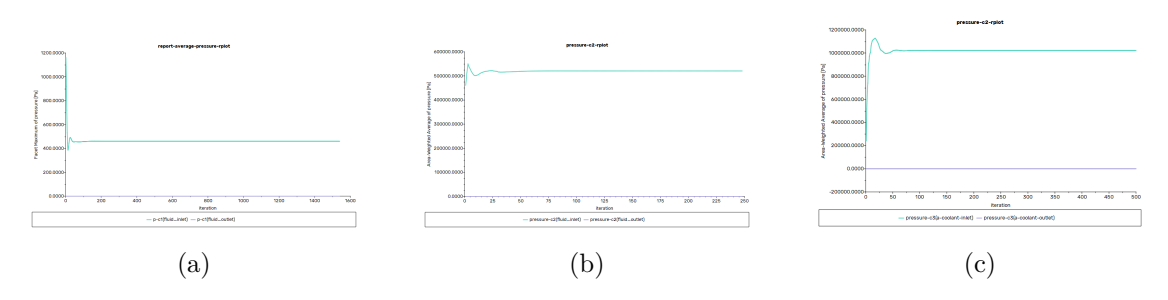


Figure 4.3: The plot of max pressure of cooling strategies: (a) Rotor shaft cooling, (b) Rotor shaft and rotor lamination cooling, and (c) Rotor shaft with direct oil-cooled magnet cooling.

4.2 Temperature

Designing an efficient cooling solution is a key step in motor thermal management. Leveraging the CFD simulation capabilities of ANSYS FLUENT, the temperature distribution patterns of various motor components can be accurately simulated. This paper analyzes the maximum temperature iteration curves derived from simulations for three different motor cooling solutions, evaluating the heat dissipation performance of each solution from various perspectives, including temperature level, convergence characteristics, and heat distribution uniformity. The curve of maximum temperature versus iteration number has dual value: first, the convergence of the curve reflects the stability of the numerical heat transfer calculations; second, the final maximum temperature value directly reflects the thermal load level of key motor components. By comparing the temperature performance of components such as magnets, windings, stator/rotor laminations, and cooling media under different solutions, the cooling efficiency and thermal management rationality of the cooling solution can be intuitively judged.

For Case 1, this solution focused on the temperature variations of core components such as the magnets, rotor laminations, stator laminations, and windings. The windings reached a maximum temperature of approximately $112^{\circ}C$, the highest temperature in this solution. The windings are the primary heat source, necessitating optimization of their cooling design. The stator-lamination system reached a maximum temperature of approximately $99^{\circ}C$, demonstrating good thermal stability. Both the magnet and rotor-lamination systems reached a similar maximum temperature of approximately $91^{\circ}C$, indicating highly uniform heat distribution on the rotor side and balanced thermal management of the rotor through the cooling solution. The simulation converged strongly, verifying the reliability of the heat transfer model; however, the winding temperatures were relatively high.

For Case 2, similar to Case 1, the highest temperature component of the motor was still the windings, at approximately $108^{\circ}C$, reflecting the heat load level of the primary internal heat source. The stator-lamination system reached a maximum temperature of approximately $94^{\circ}C$, indicating that the cooling medium effectively removed heat and that the heat exchange process achieved rapid equilibrium. The rotor-lamination and magnet systems both reached relatively low temperatures of approximately $58^{\circ}C$, demonstrating that the heat dissipation design effectively managed thermal management. Compared to Case 1, the cooling channels are closer to the heat source, effectively reducing the temperatures of the rotor lamination and magnet. However, due to the low thermal conductivity of the air gap, the temperatures of the stator lamination and winding did not change significantly with the structural design changes. This solution shows clear temperature stratification among the various components.

For Case 3, similar to Case 2, the highest motor temperature is still the winding, at approximately $108^{\circ}C$. The stator lamination reaches a maximum temperature of approximately $92^{\circ}C$, showing no significant change compared to Case 2. The rotor lamination and magnet temperatures are approximately $49^{\circ}C$, the lowest of the three solutions, demonstrating which the heat dissipation design provides the best thermal management. Compared to Cases 1 and 2, the cooling channels are closer to the heat source, covering the magnet, significantly reducing the temperatures of the rotor lamination and magnet.

However, due to the low thermal conductivity of the air gap, similar results are shown as in Case 2, with the stator lamination and winding temperatures not changing significantly with the structural design changes. This solution offers lower temperatures and more uniform heat distribution, demonstrating both balanced thermal management and reliability. The data of max temperature of each components shows in Fig.4.4 and the temperature distribution shows in Fig.4.5&4.6& 4.7:

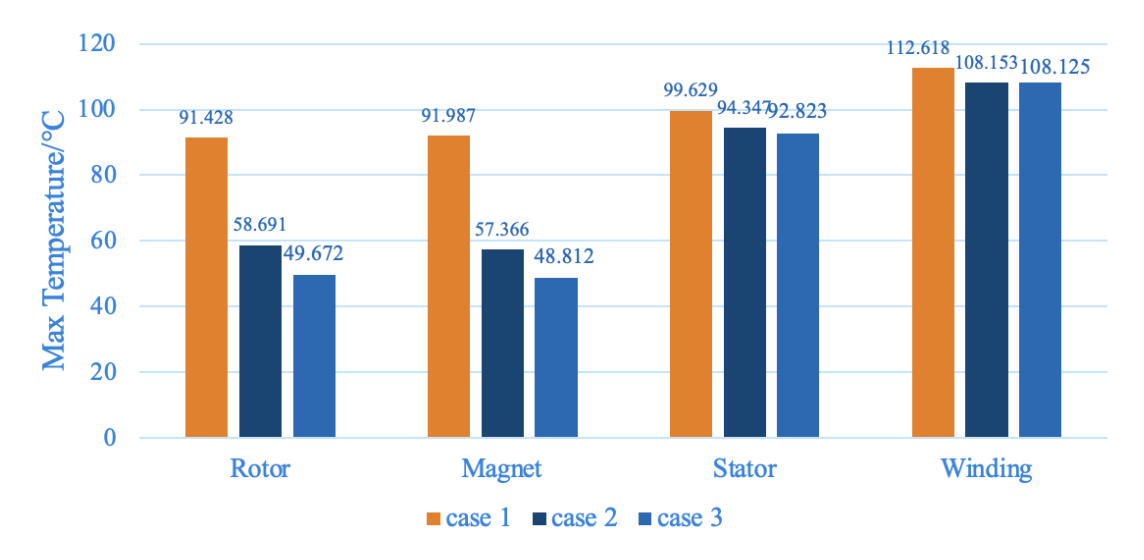


Figure 4.4: The histogram of max temperature

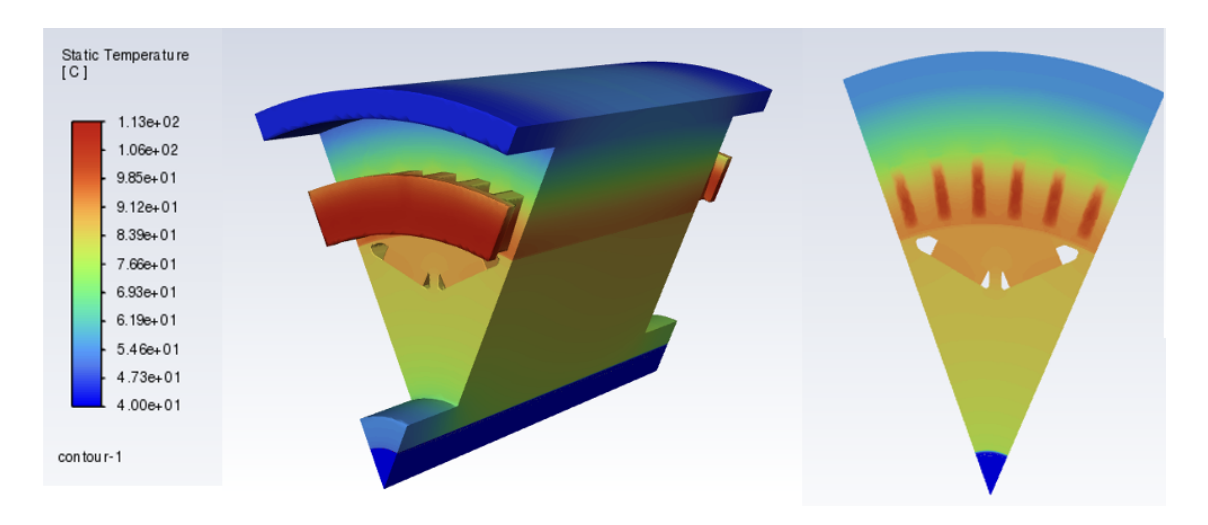


Figure 4.5: Temperature distribution and section view in the middle plane of case.1

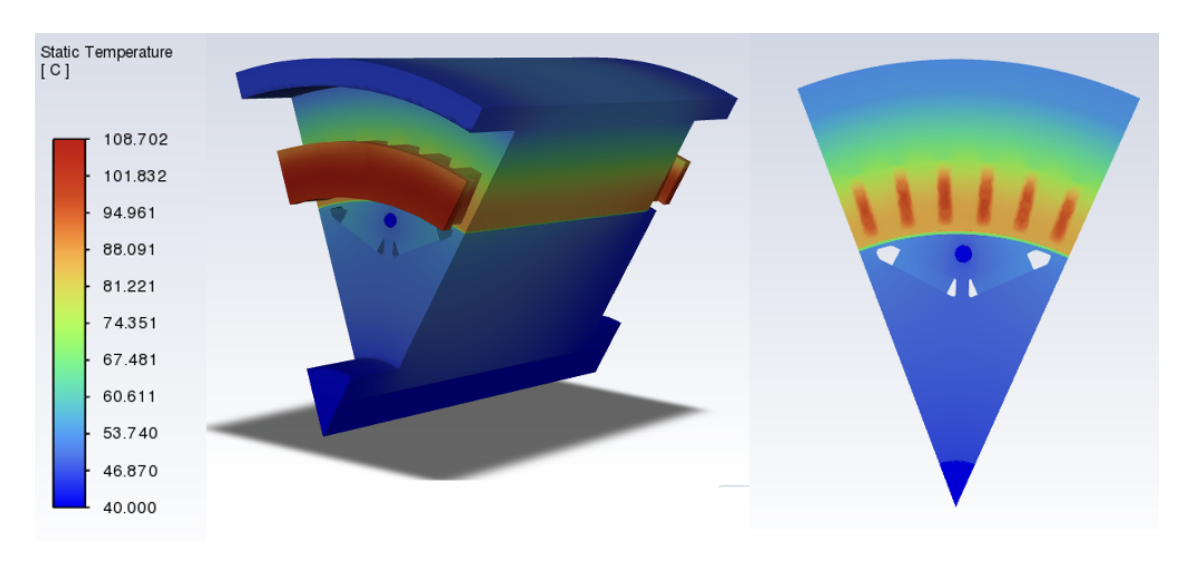


Figure 4.6: Temperature distribution and section view in the middle plane of case.2

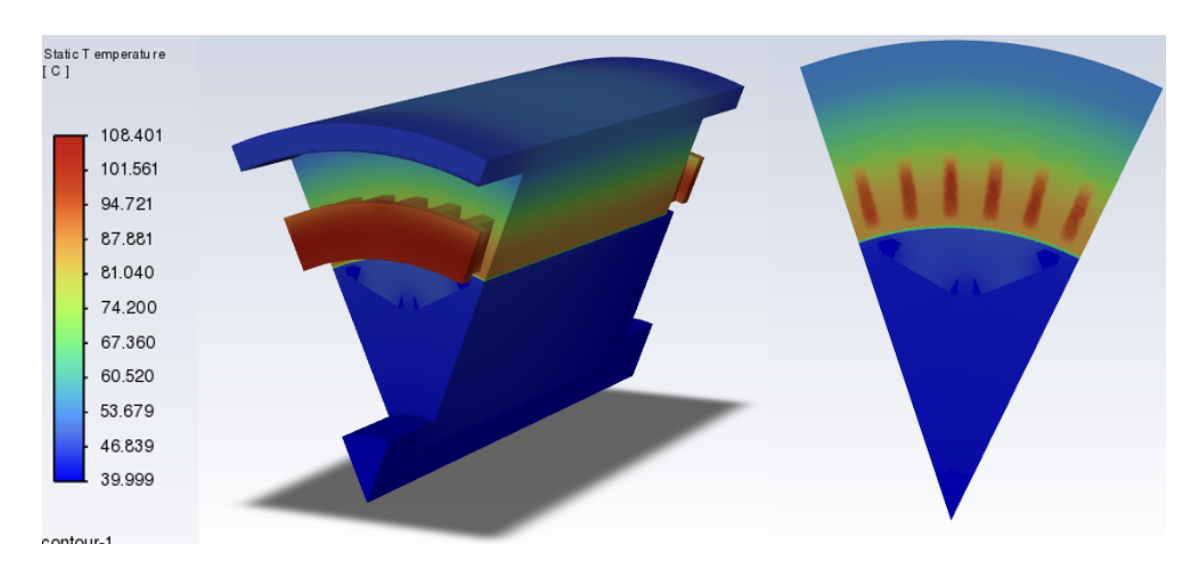


Figure 4.7: Temperature distribution and section view in the middle plane of case.3

4.3 Pressure

The pressure characteristics of the cooling medium directly affect flow power consumption and heat transfer efficiency. The lower the pressure loss, the lower the energy consumption required to drive the cooling medium. However, excessively low pressure can lead to insufficient flow and impair heat transfer. This paper analyzes the pressure iteration curves derived from simulations for three motor cooling schemes, evaluating the flow characteristics of each scheme from the perspectives of convergence, pressure level, and

pressure loss.

For Case 1, the pressure curve converges completely after approximately 200 iterations, demonstrating excellent convergence of the pressure field calculation. The pressure level, with the inlet pressure finally stabilizing at approximately 460 Pa and the outlet pressure approaching 0 Pa, results in a pressure drop of 460 Pa and minimal pressure loss.

For Case 2, rapid convergence after approximately 50 iterations demonstrates the high efficiency and stability of the pressure field calculation. The pressure level, with the inlet pressure stabilizing at approximately 520,000 Pa and the outlet pressure remaining close to 0 Pa, results in a pressure drop of approximately 520,000 Pa. Due to the narrow cooling channels in the structural design of Case 2, the pressure loss in this solution is significantly higher than in Case 1, resulting in higher driving energy consumption. However, the higher pressure can drive a larger flow rate or higher flow velocity for the cooling medium, thereby enhancing heat transfer capacity.

For Case 3, its convergence characteristics stabilize after approximately 100 iterations, with a convergence efficiency between Cases 1 and 2. The pressure level is stable at approximately 1,000,000 Pa at the inlet and 0 Pa at the outlet, with a pressure loss of 1,000,000 Pa. Due to the narrower cooling channels and more stringent design requirements in the structural design of Case 3, it has significantly higher pressure loss, resulting in higher driving energy consumption. However, it provides extremely strong flow dynamics for the cooling medium, achieving high flow rates and high flow velocities for heat transfer. The data of max pressure and driving power show in Fig.4.8&4.9:

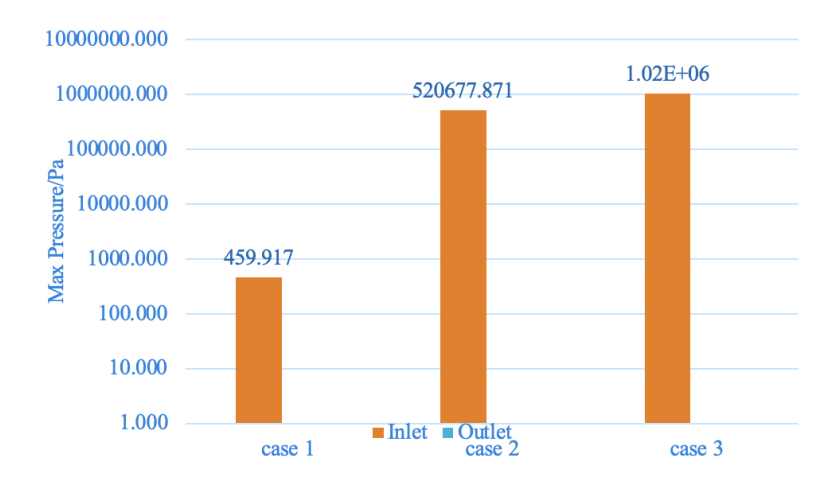


Figure 4.8: The histogram of max pressure

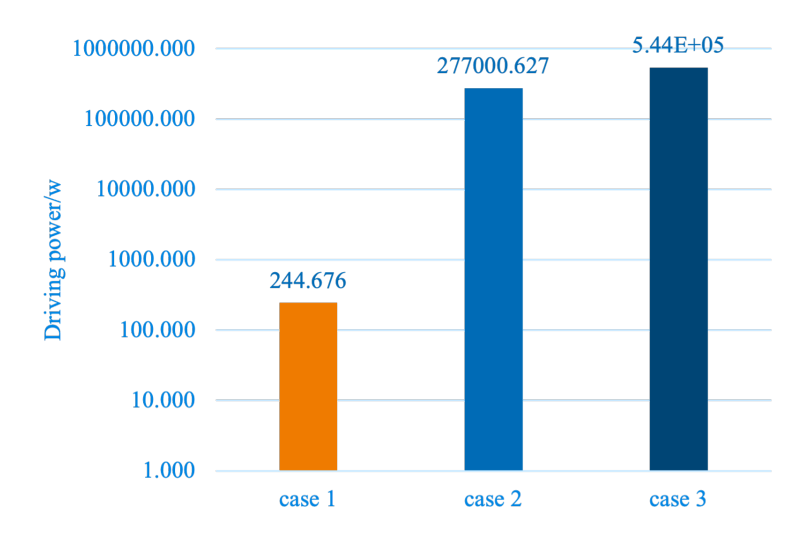


Figure 4.9: The histogram of driving power

4.4 Electric-magnetic analysis

The magnetic flux density contours.4.10 & 4.11 show that the maximum magnetic flux density for Cases 1 and 3 is approximately 2.125 T, while that for Case 2 is approximately 2.112 T, with a difference of only approximately 0.6%. The overall distribution of magnetic flux lines is highly consistent, with only a very localized flux perturbation occurring in the hole region of Case 2, which does not materially affect the continuity and uniformity of the overall magnetic circuit. Comparing the torque data, shows as Table.4.1, the differences between Cases 2 and Cases 1 and 3, both in terms of maximum possible torque and single-point torque, are within 3%, and the difference between Case 3 and Case 1 is less than 0.5%, falling within the acceptable range of minor fluctuations in engineering. Combining the magnetic field distribution and torque data reveals that local adjustments to the cooling circuit (such as the addition of cooling holes in Case 2) have minimal impact on the electromagnetic performance of motor, with the differences in magnetic flux density and torque remaining within acceptable engineering tolerances. This finding provides flexibility in motor cooling design. While ensuring thermal management requirements, local optimization of the cooling circuit (such as adding cooling holes or adjusting the flow path layout) can be performed without significantly compromising electromagnetic performance.

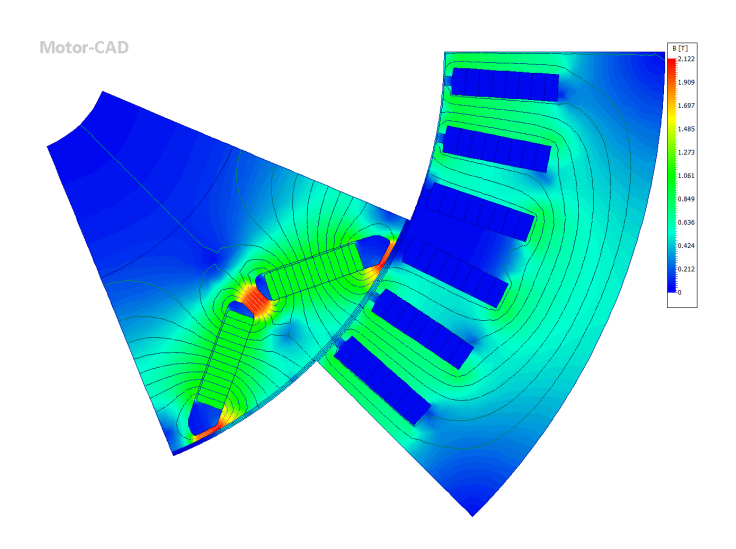


Figure 4.10: The plot of E-magnetic field of case. 1&3 $\,$

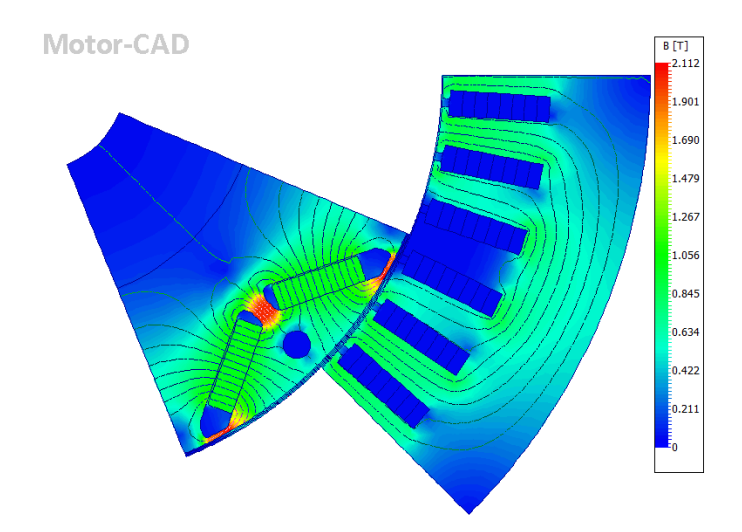


Figure 4.11: The plot of E-magnetic field of case. 2

Item	Case.1	Case.2	Case.3
Max torque possible(DQ)/Nm	87.812	86.042	87.394
Single point torque(DQ)/Nm	83.236	81.343	82.841

Table 4.1: The table of all the materials

Chapter 5

Conclusion and future work

5.1 Conclusion

The results presented in the previous section demonstrate that among the three motor cooling strategies evaluated, the third configuration achieved the best overall performance. This design significantly reduced the temperatures of the primary heat sources, including the stator windings, rotor core, and permanent magnets. The improved cooling effectiveness can be attributed to the shortened thermal path between the coolant and the heat-generating components, which facilitated more efficient heat removal from the rotor region. However, this benefit came at the cost of increased system complexity, as the associated piping design introduced a higher pressure drop. It is also noteworthy that the low thermal conductivity of the air within the air gap limited the influence of rotor cooling modifications on the thermal performance of stator. Despite these structural and thermal changes, electromagnetic analysis confirmed that the proposed cooling designs did not negatively affect the motor's electromagnetic characteristics. Overall, these findings underscore the critical role of optimized cooling channel design in enhancing the thermal performance of automotive IPM motors. The study demonstrates that targeted cooling strategies can effectively lower rotor temperatures while maintaining electromagnetic integrity, thereby contributing to the development of high-efficiency and reliable electric drive systems.

5.2 Future work

As the power density and efficiency requirements for electric vehicles, aviation motors, and high-performance industrial motors continue to increase, the importance of motor thermal management technology is becoming increasingly prominent. Future research needs to strike a balance between cooling efficiency, compactness, and cost control. Finally, future research directions include further optimizing cooling channel layout, creating a three-dimensional cooling channel network, and introducing more complex channel layouts in the rotor and stator to achieve more uniform coolant distribution. A zoned cooling strategy can be implemented, with independent cooling branches designed for different heat sources, such as windings, magnets, and bearings, to improve local heat dissipation

efficiency. Research is underway on novel cooling media, such as Nanofluid coolants, to enhance the heat transfer capacity of coolant. Phase change material-assisted cooling, by embedding phase change materials within the motor, can mitigate temperature spikes during short-term, high-power operation. Regarding multi-physics collaborative optimization, future research needs to focus on the multi-physics coupling effects of motors, optimizing cooling channel design while balancing electromagnetic performance and mechanical strength. Intelligent control cooling systems can be developed to dynamically adjust coolant flow and temperature based on the operating state, achieving a balance between energy conservation and efficient cooling. New materials and manufacturing processes are developing high-thermal conductivity stator and rotor materials, and developing laminated materials with higher thermal conductivity to reduce thermal resistance. Looking ahead at the engineering application level, future cooling designs will drive motor applications toward higher performance. In the new energy vehicle sector, this will enable higher motor power density and longer range; in the aviation motor sector, it will ensure reliable heat dissipation in extreme high-altitude, low-pressure environments; in the high-speed motor sector, it will support thermal stability at speeds in the 10,000 rpm range; and in industrial scenarios, it will improve the reliability and cost-effectiveness of long-term operation.

List of Figures

2.1	$k-\omega$ SST model switches between $k-\epsilon$ and $k-\omega$ turbulence model [7].
2.2	Fin configuration geometry [3]
2.3	Ventilation structure of an EFC motor [3]
2.4	Forced-liquid cooling model [3]
2.5	Wet stator cooling system [3]
2.6	Indirect rotor cooling scheme $[3]$
2.7	Primary components of a phase change cooling loop [3]
3.1	Axial cross view of cooling strategies: (a) Rotor shaft cooling, (b) Rotor shaft and rotor lamination cooling, and (c) Rotor shaft with direct oil-cooled magnet cooling. Arrows denote the fluid flow
3.2	Radial cross view of cooling strategies: (a)case.1&3(b)case.2
3.3	3D geometric model of case.1
3.4	3D geometric model of case.2
3.5	3D geometric model of case.3
3.6	Periodic boundary conditions: (a) Rotational periodic boundary surface of one-eighth motor.1(b)Rotational periodic boundary surface of one-eighth motor.2
3.7	Winding cross section
3.8	Thermal resistant layout
3.9	Curvilinear coordinate system for winding
3.10	Equivalence of the Rotor and Air-gap
3.11	Equivalence of the housing wall
3.12	The total loss map
3.13	The iron loss map
3.14	The rotor back iron loss map
3.15	The stator back iron loss map
3.16	The magnet loss map
3.17	The copper loss map
4.1	The plot of residual of cooling strategies: (a) Rotor shaft cooling, (b) Rotor shaft and rotor lamination cooling, and (c) Rotor shaft with direct oil-cooled magnet cooling

List of Figures

4.2	The plot of max temperature of cooling strategies: (a) Rotor shaft cooling,	
	(b) Rotor shaft and rotor lamination cooling, and (c) Rotor shaft with	
	direct oil-cooled magnet cooling	41
4.3	The plot of max pressure of cooling strategies: (a) Rotor shaft cooling, (b)	
	Rotor shaft and rotor lamination cooling, and (c) Rotor shaft with direct	
	oil-cooled magnet cooling.	41
4.4	The histogram of max temperature	43
4.5	Temperature distribution and section view in the middle plane of case. 1 .	43
4.6	Temperature distribution and section view in the middle plane of case. 2 .	44
4.7	Temperature distribution and section view in the middle plane of case. 3 .	44
4.8	The histogram of max pressure	45
4.9	The histogram of driving power	46
4.10	The plot of E-magnetic field of case.1&3	47
4.11	The plot of E-magnetic field of case.2	47

Bibliography

- [1] Yew Chuan Chong, Saeed Jahangirian, Husain Adam, Melanie Michon, Chuan Liu, Zeyuan Xu, David Gerada, and Chris Gerada. Analytical modelling technique of oil-cooled electric machine using empirical correlation and lptn. In 2023 IEEE International Electric Machines & Drives Conference (IEMDC), pages 1–7, 2023.
- [2] European Environment Agency. Electric vehicles, 2023. Accessed: 2025-09-24.
- [3] Yaohui Gai, Mohammad Kimiabeigi, Yew Chuan Chong, James D. Widmer, Xu Deng, Mircea Popescu, James Goss, Dave A. Staton, and Andrew Steven. Cooling of automotive traction motors: Schemes, examples, and computation methods. *IEEE Transactions on Industrial Electronics*, 66(3):1681–1692, 2019.
- [4] Marklines. Automotive sales in china by month, 2025. Accessed: 2025-09-24.
- [5] Ministry of Industry and Information Technology of China. Production and sales of new energy vehicles in the first half of 2025, 2025. Accessed: 2025-09-24.
- [6] Reuters. Battery electric cars produce 73% less emissions research. Reuters Sustainability, 2025. Accessed: 2025-09-24.
- [7] SimScale. K-omega turbulence models | global settings. https://www.simscale.com/docs/simulation-setup/global-settings/k-omega-sst/. Accessed: 2025-10-02
- [8] U.S. Department of Energy. Electric vehicle emissions, 2024. Accessed: 2025-09-24.
- [9] U.S. Environmental Protection Agency. Electric vehicle myths, 2024. Accessed: 2025-09-24.